

Review

ORR Catalysts Derived from Biopolymers

Jelena Rupar ¹, Danijela Tekić ², Aleksandra Janošević Ležaić ¹ and Kush K. Upadhyay ^{3,*}

¹ Department of Physical Chemistry and Instrumental Methods, University of Belgrade—Faculty of Pharmacy, 11221 Belgrade, Serbia

² University of Belgrade—Faculty of Physical Chemistry, 11158 Belgrade, Serbia

³ Centro de Química Estrutural-CQE, Departamento de Engenharia Química, Instituto Superior Técnico, Universidade de Lisboa, 1049-001 Lisboa, Portugal

* Correspondence: kush.upadhyay@c2cnewcap.com or kushkumar434@gmail.com

Abstract: Due to the limited reaction rate of the oxygen reduction reaction (ORR), it is considered as a limiting factor in the performance of fuel cells and metal-air batteries. Platinum is considered the benchmark catalyst for ORR; however, the scarcity of platinum, its high price, the drift phenomenon, its insufficient durability, and its susceptibility to gas poisoning are the reasons for the constant search for new ORR catalysts. Carbon-based catalysts show exceptional promise in this respect considering economic profitability and activity, and, in addition, they have favorable conductivity and often a large specific surface area. The use of chitin, cellulose, lignin, coconut shell particles, shrimp shells, and even hair for this purpose was reported, as they had similar electrochemical activity regarding Pt. Alginate, a natural polymer and a constituent of brown algae, can be successfully used to obtain carbon materials that catalyze ORR. In addition, metal atomic-level catalysts and metal N-doped porous carbon materials, obtained from sodium alginate as a precursor, have been proposed as efficient electrocatalysts for ORR. Except for alginate, other biopolymers have been reported to play an important role in the preparation of ORR catalysts. In this review, recent advances regarding biopolymer-derived ORR catalysts are summarized, with a focus on alginate as a source.

Keywords: oxygen reduction reaction; biopolymers; alginate; carbon porous catalysts



Citation: Rupar, J.; Tekić, D.; Janošević Ležaić, A.; Upadhyay, K.K. ORR Catalysts Derived from Biopolymers. *Catalysts* **2023**, *13*, 80. <https://doi.org/10.3390/catal13010080>

Academic Editor:
Nicolas Alonso-Vante

Received: 30 November 2022
Revised: 17 December 2022
Accepted: 25 December 2022
Published: 30 December 2022



Copyright: © 2022 by the authors. Licensee MDPI, Basel, Switzerland. This article is an open access article distributed under the terms and conditions of the Creative Commons Attribution (CC BY) license (<https://creativecommons.org/licenses/by/4.0/>).

1. Introduction

In recent years, the awareness of the human influence on climate change has increased. More and more attention is being paid to factors leading to global warming, especially CO₂ emissions. As fossil fuel usage leads to CO₂ release into the atmosphere [1], in addition to their limited availability [2], research groups worldwide are dedicated to finding alternatives to the carbon cycle. Fuel cells are of extraordinary importance in this respect, as they can participate in the hydrogen cycle. Fuel cells, as devices that convert oxygen and chemical energy into electricity with a high efficiency, are considered environmentally friendly and can be used for small, portable electronic devices and military and space devices [3–5]. Metal-air batteries represent cost-effective devices that require an air atmosphere [6], and the most promising are Zn-air batteries, with a high theoretical energy density, solid rechargeability, and flat discharge voltage [7,8]. During discharge, the reduction of oxygen at the cathode occurs while the metal oxidizes and releases electrons which pass through the external circuit in metal-air batteries. In the fuel cells, the H₂ dissociation occurs at the anode, while at the cathode, O₂ reduction occurs, transforming chemical energy into electricity [9]; thus, oxygen reduction reaction (ORR) is the most important cathode reaction for both types of devices [10–12].

The ORR catalyst is the main descriptor for the performance of these devices, with conventional platinum still regarded as the best ORR catalyst in both acid and alkaline electrolytes. However, Pt has a high price, a susceptibility to time-dependent drift, and

serious anode crossover, and it is easily poisoned by CO (an intermediate product of electro-oxidizing alcohol fuels), which limits its usage. The limited availability of Pt is another important fact and constrains the possibility of using devices whose operation is based on ORR [13,14]. Therefore, platinum has to be replaced with appropriate alternatives that have a similar catalytic activity and can be produced massively and cost-effectively from Earth's abundant resources [15]. Electrocatalysts should have high electrical conductivities, large specific surface areas, and electroactive properties [11,16]. Conductive polymers (CPs) and carbon materials (grapheme, carbon nanotubes (CNTs), amorphous carbon, and carbon nanofibers) can fulfil these requirements, and they have been widely explored for oxygen reduction in fuel cells, among other applications [13,17].

CPs that have been found to be useful as ORR catalysts can be classified into three groups: inherent CPs, CP-derived heteroatom-doped carbons, and CP composites. The activity of inherent CPs is a consequence of their structure, so the transfer of electrons with oxygen in molecular form occurs due to the characteristic that the neutral CP is an electron donor for O_2 , while O_2 is an electron acceptor. Adsorbed oxygen on the CP surface accepts an electron, and its molecular symmetry decreases while the length of the $O = O$ bond increases. In addition, due to the reaction with adsorbed oxygen molecules, the CPs that are mildly oxidized transform to a higher oxidation state, while the oxygen molecules are reduced into O^{2-} anions [17,18]. As many research groups directed their research interest towards the development of ORR catalysts from CPs, it was established that catalytic performances can be improved if a metal is incorporated into the CP [19] or if the CP is doped with a heteroatom. When Dai et al., in 2009, reported the strong ORR catalytic activity of carbon nanotubes doped with nitrogen, a new research field for N-doped carbon catalysts investigation was opened [17–20]. In addition to monoatomic doping, co-doping with other heteroatoms (B, O, S, P) proved to be an important direction for the synthesis of ORR catalysts, taking into account the increase in the asymmetrical spin density obtained in that case [21–23]. While B- and P-doped carbon without N-doping mainly enabled ORR via a two-electron process [24,25], B,N-doped carbon was proposed as an ORR catalyst, indicating a four-electron ORR in alkaline media [26]. In acidic media, the co-doping of N-doped material with only B influenced the increase in H_2O_2 production, and additionally doping it with P decreased the production of H_2O_2 , consequently leading to it favoring the four-electron process [21]. Zhang et al. [22] designed N and P co-doped material by using polyaniline pyrolysis and developed the ORR OER dual catalyst, which enables the reduction to occur via the four-electron pathway.

For tridoped nanoporous carbon material with N-, O-, and S-, it was suggested that the O_2 molecule was reduced via a four-electron process in 0.1 M KOH solution. Compared to metal-based catalysts, this material had improved the catalytic activity; thus, it influenced the growth of research in this area [23].

Additionally, it was reported that the incorporation of transition-metal active centers had an influence on the electrocatalytic activity [27–30]. Transition metals such as Mn, Fe, Co, Ni, etc. have empty 3d orbitals; thus, they can accept an electron and have the ability to reduce the bonding energy between OOH^* , O^*/OH^* intermediates [31,32]. As facilitating the O-O bond breaking in OOH^* leads to the inhibition of H_2O_2 formation, this material quality is important for improving the four-electron ORR pathway selectivity [33].

Published materials [34] containing Fe [35], which had an electrocatalytic activity comparable to Pt/C in alkaline as well as in neutral and acidic medium, with an electron transfer number of about 4. Additionally, there is evidence that the introduction of two transition metals instead of one enhances the four-electron pathway selectivity [31].

Yang et al. [31] synthesized a binuclear catalyst containing Fe and Mn with excellent four-electron pathway selectivity in acidic media [34].

In accordance with the above, the heteroatom-doped carbon and transition metal coordinated by N in the carbon network are considered as the most promising catalysts for ORR [13].

The porous structure is an important parameter for the platinum group metal (PGM)-free ORR catalysts. Micropores host the majority of the active sites, while the mesopores primarily have the role of the mass transfer channel. Thus, the electrocatalytic activity is determined by micro- and mesoporosity [13,36].

The materials derived from biomass can inherit the macro-, meso-, and microporosity of the original biological precursors well after appropriate conversion processes [13,37–39].

The carbonization temperature presents another important factor that affects the activity of the bio-based carbon catalyst. As the temperature increases, the graphitization degree increases from about 75% to about 85%, and the electrical conductivity also increases [40,41]. In addition, the temperature increase leads to porosity development [36]. Additionally, the activity of the carbon-based catalyst depends on the relationship between the electron conductivity and the specific surface area. However, many works do not contain information about the specific surface area. The future is certainly represented by carbon foams with a system of open pores that enable the highest availability of active sites for oxygen and thus improve catalytic activity.

The defects of different sorts had a great influence on the ORR mechanism in the alkaline medium, while in the acidic medium, the influence was less pronounced [42]. Additionally, there is evidence that the rate of heteroatom influenced the catalytic activity; a higher content of heteroatom leads to an increase in structural defects and improves catalytic activity [43]. The researchers agree on the fact that the level of nitrogen influences the electrocatalytic activity. While increasing the level of nitrogen content, the ORR activity increases. The performance improvement is primarily due to the presence of free-flowing sp^2 -hybridized π electrons. In addition, the presence of free electron pairs of nitrogen atoms contributes to the bonding of the delocalized carbon matrix system, thereby further improving the electrocatalytic activity of ORR to a large extent. It is also known that heteroatoms doping can enhance the catalytic activity given that the doped heteroatom generally has the greater electronegativity compared to carbon atoms; this induces a partial positive charge near the carbon atoms and enhances the ORR [44,45]. The problem arises when the influence of the nitrogen type is discussed, since it is not entirely clear which nitrogen functional groups had a direct effect on the catalytic activity.

Various loadings of carbon-based materials in the range between 0.10 and 1.00 mg/cm² [46,47] were tried, and its influence on ORR was assessed. The results showed that low-carbon loadings were not sufficient in covering the electrode surface and consequently led to lower current densities and, predominantly, the $2e^-$ mechanism. With an increase in loading up to around 0.25 mg/cm², higher currents were measured, with a shift in the mechanism towards $4e^-$ reduction. A further increase in loading was detrimental to the ORR performance of carbon-based materials. An explanation for this occurrence is the excessively long electron path caused by the catalyst layer thickness, which results in substantial electrical resistance and mass transport losses. Both phenomena limited the access to some of the electroactive sites, independent of the sites' actual activity towards ORR. Film thickness also affects the total available surface area as well as the materials' bulk density, so there exists a trade-off between all these different effects when considering the overall ORR performance. Lastly, layer thickness seems to have an effect on the ORR mechanism itself by increasing the number of apparently exchanged electrons with the increase in loading. Namely, thicker layer intermediates, such as OOH^- , remain near the carbon surface for longer periods of time and participate in the second $2e^-$ reduction to OH^- [46,48], pushing the number of electrons towards four. This phenomenon is more pronounced for materials with sites of higher activity.

It is of particular importance to mention that ORR catalysts can also be synthesized using biogenic precursors. The authors Ye et al. [49] presented a synthesis process of ORR catalysts containing Fe-P active centers. After the carbonization of the biogenic precursor, i.e., the bacteria@vivianite composite, which was obtained due to the reduction of polyferric flocs by *Shewanella oneidensis* MR-1, the obtained material showed an excellent catalytic activity. Chitin, as the most abundant natural nitrogen-containing compound, is an ideal

precursor for the synthesis of ORR catalysts using only a high temperature, without additional dopants [50,51]. Human hair, consisting of keratin, with contents of about 15–16% nitrogen and 4.5–5.5% sulfur [52], may also be used as a biogenic precursor for obtaining heteroatom-doped carbon material through the process that uses no hazardous reagents [53].

Biopolymers, substances consisting of numerous repeating monomer units, are present in natural sources. In Table 1, the principal advantages and disadvantages of natural biopolymers are presented [54,55]. These are promising candidates for different spheres of medicine and industry due to their biocompatibility and biodegradability. The biopolymers are used as edible films, emulsions, packaging materials in the food industry, drug transport materials, medical implants, tissue scaffolds, dressing materials in pharmaceutical industries, etc. [55].

Table 1. The positive and negative aspects of natural biopolymers.

Positive Aspects	Negative Aspects
biologically renewable	low melting point
biodegradable	less stable
biocompatible	structurally more complex
non-toxic	high surface tension
biofunctional	

In this review, we will discuss the use of some biopolymers-based materials as promising candidates for ORR catalysis, whose performance was most often tested in alkaline conditions. Those that are applied most often are alginate, cellulose, chitin, and lignin due to their broad availability and low price [56–61].

Figure 1 represents the biopolymer categorization [55] with respect to the biopolymers considered in this review paper.

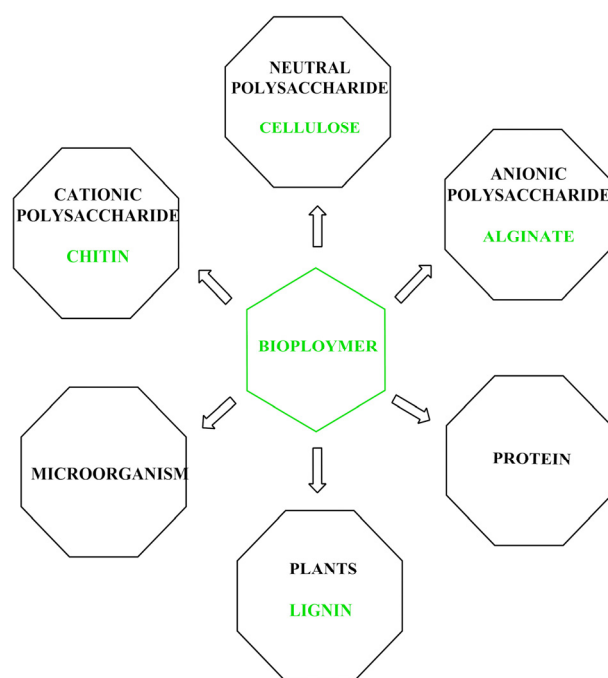


Figure 1. A pictorial depiction of several natural, renewable biopolymers categorized according to their source [55].

In Table 2, the structures of the biopolymers reviewed in this paper are presented.

Table 2. Main biopolymers and their chemical structures [62].

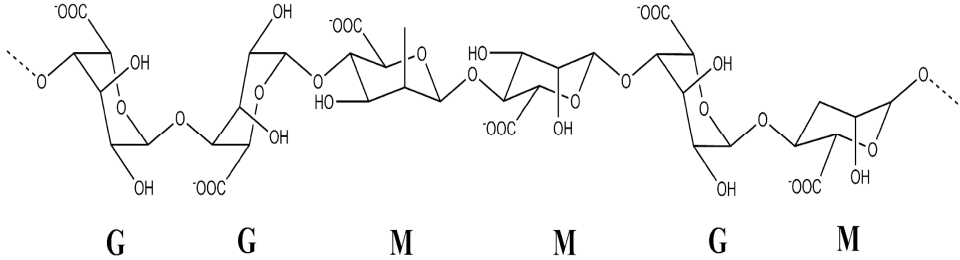
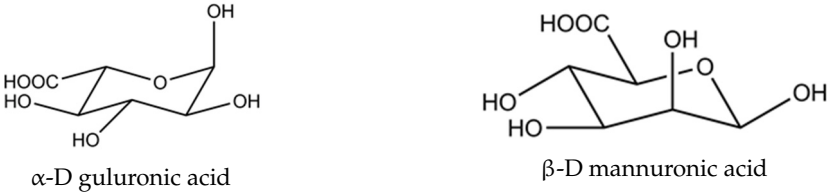
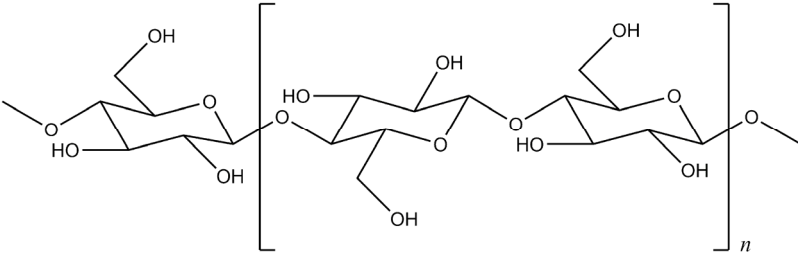
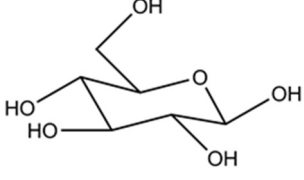
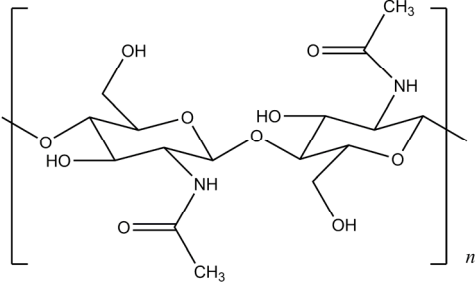
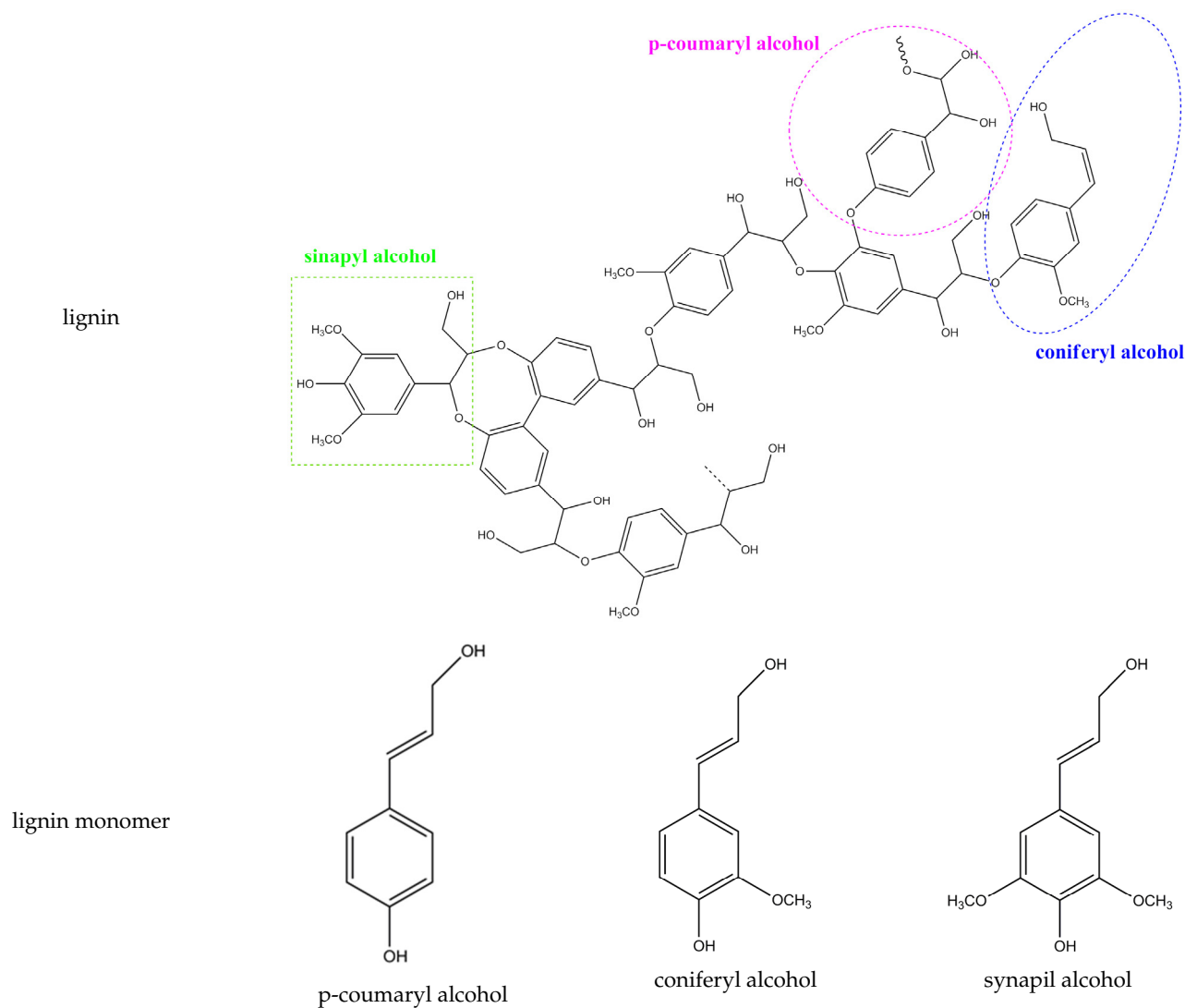
alginate	 <p style="text-align: center;">G G M M G M</p>
alginate monomer	 <p style="text-align: center;">α-D guluronic acid β-D mannuronic acid</p>
cellulose	
cellulose monomer	 <p style="text-align: center;">glucose</p>
chitin	 <p style="text-align: center;">N-acetylglucosamine</p>

Table 2. Cont.



Major challenges during the synthesis of ORR catalysts include the efforts to extract biopolymers from the biomass, along with methods for cleaning and decomposition, simplifying the conversion processes with the aim of ensuring the low cost of synthesis and production on a bigger scale. Knowledge of active sites and the relationship between the structure and mass transfer can facilitate the selection of materials and the methodology for ORR synthesis. Additionally, it is necessary to intensively transfer the half-cells tests of synthesized ORR catalysts to corresponding devices, such as fuel cells and metal-air batteries [13].

2. Alginate as a Source of Carbon Material

Biopolymers, as renewable and non-toxic precursors, are important for the synthesis of carbon materials. Abundant sea resources represent one of the most important sources, considering that the ocean occupies three-quarters of the Earth's surface [63].

The wide alginates availability, with the simplicity of their extraction and synthesis via "green" processes, makes them exceptionally favorable materials, both commercially and environmentally. The field of their applications and significance is expanding, and one of the main challenges is their use as precursors of carbon materials production on a large scale.

Brown algae are a valuable source of alginate, a natural polymer composed of β -D-mannuronate and α -L-guluronate. Due to the structure, as alginate consists of a large number of carboxyl and hydroxyl groups in the polymer chain, it is possible to obtain porous carbon material after alginate carbonization [64,65]. However, the different sequence and structure that vary depending on the source may be a disadvantage when this biopolymer is used [66]. Alginate interacts with metal ions and can chelate divalent and trivalent ions such as Ca^{2+} , Co^{2+} , Ni^{2+} , Zn^{2+} , and Fe^{3+} , consequently forming an “egg-box” structure that can be used for the synthesis of metal-doped/free three-dimensional carbon nanomaterials with multimodal pores. This represents one of the main advantages of using the alginate as a precursor considering that the 1D structure has a very pronounced limited mass transfer of electrolyte ions. Multimodal pores formation was reported as a result of the material acid rinsing after thermal treatment in an inert gas atmosphere [67,68]. Large pores corresponded to the elimination of metal chelated into alginate, while smaller pores were the result of the release of H_2O and CO_2 during the thermal treatment.

Li et al. developed N-doped porous graphitic carbon nanofibers (N-PCNFs) with multimodal pores by the pyrolysis of electrospun alginate nanofibers at different temperatures (Figure 2). The result of the annealing treatment at 600 °C in ammonia was the formation of a metal-free catalyst for ORR with a higher stability and methanol tolerance for ORR in comparison to Pt/C. The mechanism revealed the four-electron pathway in an alkaline solution, with a capacity of 625 mAh g⁻¹ [63]. Porous graphitic carbon nanofibers without N were also prepared via the pyrolysis of alginate. However, N-doping influenced the formation of defective structures in the carbon framework with a specific area of 283 m² g⁻¹, implying increased active sites and an enhanced electrochemical performance. Based on the Koutecky–Levich (K-L) plots, the electron transfer number was calculated. At 0.4 V, the *n*-value was 3.95, indicating that the catalyst ensures that the reduction mechanism takes place as a four-electron mechanism. Voltametric studies were employed, and cyclic voltammograms of N-PCNFs showed a well-defined reduction peak (at about 0.76 V vs. RHE), which indicated oxygen reduction. Linear sweep voltammetry (LSV) was also applied in an O₂-saturated 0.1 M KOH solution with a rotating disk electrode (RDE), and the ORR onset potential and half-wave potential of N-PCNFs-600 were 0.953 and 0.810 V, respectively. In 0.5 M H₂SO₄, the onset potential was 0.55 V, while the half-wave potential was 0.35 V. Chronoamperometric measurements were conducted at 0.70 V with a rotating speed of 1600 rpm with the aim of evaluating the methanol tolerance, whereby N-PCNF-600 had a better fuel selectivity toward ORR than Pt/C considering that the current density was stable after the addition of methanol. The durability was examined at a constant voltage of 0.3 V for 15 h in an 0.1 M KOH solution at a rotation rate of 1600 rpm. The synthesized catalyst had a slower decrease of 16% than Pt/C (25%) and, thus, a better durability.

The high charge and discharge performance, based on the specific structure and bimodal shape of the pore size distribution, is one of the important advantages of this catalyst.

Zhao et al. used calcium ions to form a network with alginate, after which wet spinning was applied with the aim of obtaining calcium alginate fibers (CAFs). CAFs were treated with an acid solution to remove metal ions [69,70], and the remaining carbon fibers were used for further experiments. N and S atoms from thioacetamide were doped into carbon fibers during pyrolysis, and after annealing at 1000 °C, the recombinant carbon atoms formed a metal-free structure without S and N atoms with defects (D-CFs), which aimed to improve the catalytic activity for ORR [71–73]. D-CFs had micro- and mesopores which enabled the availability of active sites and facilitated the transport of the reaction participants with a specific surface area of 485.2 m² g⁻¹ and a 795 mAh g⁻¹ capacity [74]. The initial potential was 0.92 V vs. RHE in 0.1 KOH, and the limiting current density was 5.38 mA cm⁻², which were comparable to those of Pt/C. The half-wave potential was 0.84 V vs. RHE, equivalent to that of Pt/C in 0.1 M KOH. The reaction process catalyzed by D-CFs was determined to take place as a four-electron pathway at 0.25, 0.35, and 0.45 V vs. RHE. By comparing D-CFs and Pt/C, the chronoamperometric results confirmed the better

methanol tolerance that was expected. After 10 h, the current density for D-CFs was 94%, compared to 87% for Pt/C [70].

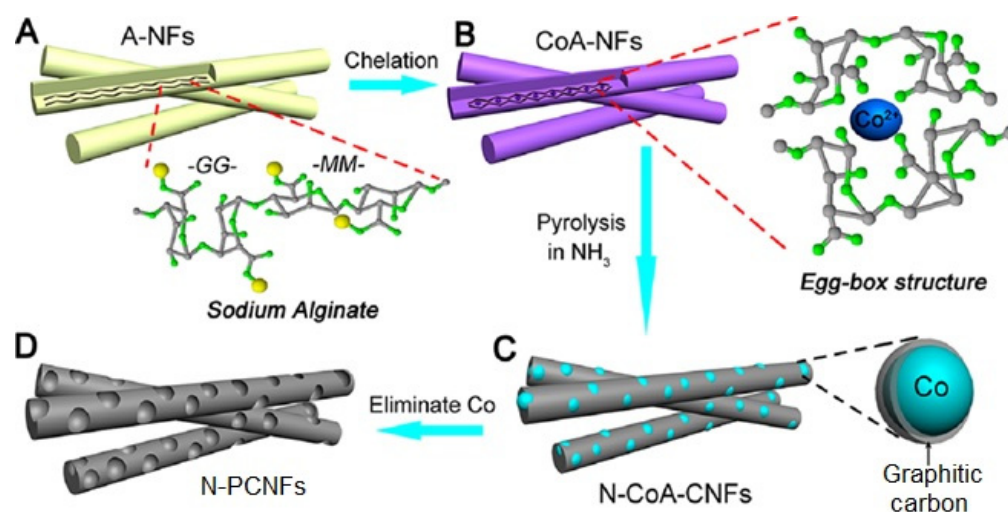


Figure 2. Schematic illustration of the synthesis process of N-doped porous graphitic carbon nanofibers (N-PCNFs). Reprinted from [63] with permission. Copyright 2015 American Chemical Society.

Considering the characteristics mentioned in the paper and the low cost, the obtained material could find its usage in large-scale applications of zinc-air batteries.

Alginate-Based Materials Doped with Metal Ions

Shu et al. [75] reported a novel strategy, thus broadening the methodology for the synthesis of Co/N-doped hierarchical porous carbon microspheres (Co/NHPCMS) with ZIF-67 (zeolite imidazolate framework), which were grown on the carbon frameworks. During the synthesis, ZIF-67 nanocrystals were grown on a carbon framework, and they improved the catalytic activity considering that they represent an in situ source of nitrogen for the material doping [76]. Sodium alginate/NaHCO₃ (SA/NaHCO₃) solution as a precursor and the electrospinning technique were used to form Co-SA/NaHCO₃ hydrogel microspheres. The specific structure of the alginate enabled the formation of a 3D network which improved the mass/charge transfer and increased the density of active sites. In such a structure, Co²⁺ formed an “egg-box” model and acted as the metal source of ZIF-67. ZIF-67@SA/NaHCO₃ microspheres were pyrolyzed in the nitrogen atmosphere, and Co/NHPCMS was obtained, with a specific surface area of 252 m² g⁻¹. For comparison, the same procedure was performed without NaHCO₃, and the ORR activity test showed that NaHCO₃ contributes to better ORR catalytic activity considering that the decomposition of NaHCO₃ results in the formation of more pores and defects, which increase the density of active sites. According to the XPS spectrum, the pyridinic and graphitic-N were considered as active sites. Additionally, it was suggested that pyridinic nitrogen could coordinate with cobalt ion. The Co nanoparticles influenced the aggregation process and corrosion and improved the stability of the catalyst [75,77].

The LSV-obtained data included the half-wave potential, which was 0.827 V, close to that of commercial Pt/C (0.851 V). Such positive values indicated a great advantage of the hierarchical porous structure. The K-L plots gave a linear dependence, and the electron transfer number was greater than 4, probably as a result of the adopted values for the K-L equation being different from the ideal. According to the chronoamperometric measurement, in O₂-saturated 0.1 M KOH at a potential of 0.6 V (vs. RHE), at a rotation rate of 1600 rpm, the relative current decreased to 79.10% after 18,000 s. Thus, compared to Pt/C, the newly synthesized catalyst showed greater ORR stability. Co/NHPCMS was

also more tolerant to methanol compared to commercial Pt/C, as no change in the current density was observed after 200 s, when 1 mL of methanol was added [75].

Ma et al. [78] developed a novel hybrid material, a three-dimensional nanostructured electrocatalyst, for ORR and OER by the pyrolysis of (Ni,Co)/carbon nanotubes (CNTs) alginate hydrogels. SA/CNTs aqueous solution (Figure 3a,d) was exposed to a solution containing Co^{2+} and Ni^{2+} ions to form an "egg-box structure" (Figure 3b,e). Upon obtaining hydrogels, the freeze-drying process was used to form (Ni, Co)-alginate/CNT aerogels (Figure 3c,f). Carbonization in the NH_3 atmosphere was conducted in order to obtain the final form of the catalyst, whereby the catalyst Ni/NiO/NiCO₂O₄-N-CNT-As (As-aerogels) showed a significant advantage in terms of catalytic properties in comparison with commercial Pt/C, with a surface area of 222 m² g⁻¹. The high activity of CNTs was explained as a result of the possibility of pyridinic and graphitic nitrogen exerting an electron on the encapsulated Co nanoparticles [14,65,79]. Accordingly, the catalytic activity was attributed to the ternary Ni/NiO/NiCO₂O₄ active site for electron transfer and the 3D hierarchical mesoporous hybrid network for mass transport. The onset potential and half-wave potential of Ni/NiO/NiCO₂O₄-N-CNT-As (obtained by LSV) were 0.89 V and 0.74 V vs. RHE, respectively, compared to 0.92 V and 0.78 V for Pt/C. Based on the reviewed results, newly synthesized catalysts were recommended as ORR catalysts, especially as bifunctional for ORR and OER. According to the N₂ adsorption-desorption isotherms and BJH pore size distribution, the synthesized material had a bimodal shape in the pore size distribution, large mesopores as a consequence of interconnected voids from tangled CNTs in the aerogels, and small mesopores as a consequence of H₂O and CO₂ release [79].

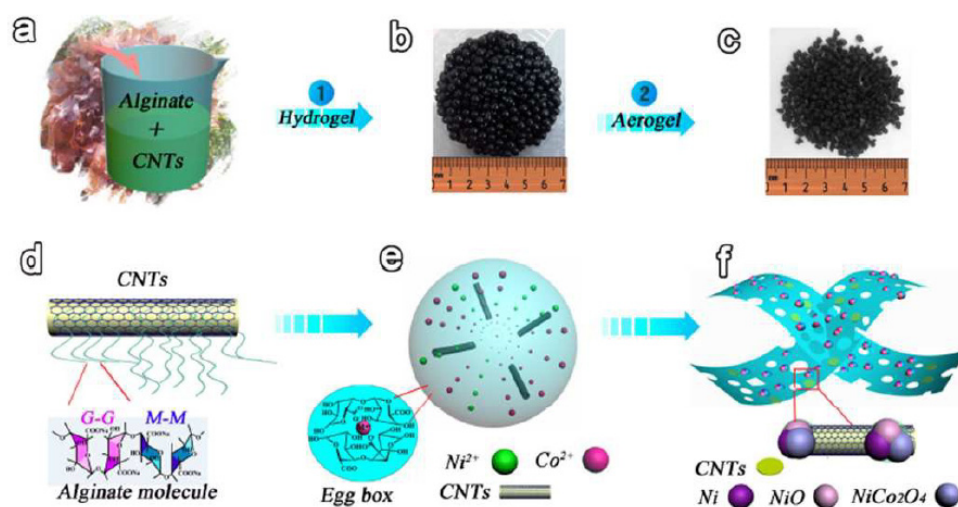


Figure 3. Schematic synthesis of Ni/NiO/NiCo₂O₄/N-CNT-As electrocatalysts; (a,d) schematic representation of SA with CNs, (b,e) hydrogels formed upon addition of aqueous solution containing Co^{2+} and Ni^{2+} ions; (c,f) freeze-dried hydrogels formed aerogels. Reprinted with permission from [78]. Copyright 2015 The Royal Society of Chemistry.

According to the K–L equation, as in other reported materials in this review, the number of electrons was 3.8, a value desirable for ORR. The durability was tested at a constant voltage of 0.69 V vs. RHE for 22,000 s at a rotation rate of 1600 rpm, where the current loss was 9%, proving the improved durability compared to commercial Pt/C. Additionally, the tolerance to methanol was better for the Ni/NiO/NiCO₂O₄-N-CNT-As, as the negative current appeared after the introduction of O₂ in the KOH saturated with N₂ at 1000 s, while subsequently, after the addition of 3M methanol, the newly synthesized catalyst's current had no changes [78].

The proposed method may be easily large-scaled, so it presents a valuable reference for the formation of dual ORR and OER catalysts.

Zhang et al. [80] developed a catalyst consisting of a 3D N-doped porous carbon matrix with $\text{Co}_3\text{O}_4/\text{Co}$ active species– $\text{Co}_3\text{O}_4/\text{Co}$ -NPC and a uniform porous nanostructure with a surface area of $496.4 \text{ m}^2 \text{ g}^{-1}$. The great advantage of the developed method was certainly the simple and low-cost synthesis, as they used hydrothermal reaction, unlike methods that use an electrospun technique or complex procedures. This method is one of the most promising methods for the synthesis of ORR catalysts [81–85]. In addition to catalyzing the ORR, the catalyst can be used for anodic oxygen evolution reaction (OER) as well; thus, it possibly has practical applications for energy conversion.

Carbon materials contributed to a better stability and conductivity and an increased surface area compared to the nanostructures of cobalt oxides and/or hydroxides [86–89]. Nevertheless, hybrid material consisting of metal at the nanoscale and heteroatom co-doped carbon showed better performances as ORR catalysts and bifunctional ORR/OER catalysts [90,91]. As biopolymers provide a cost-effective and renewable source, they attracted the attention of these authors as well [80]. After the chemical reaction of SA with Co ions, SA formed a network such that, after carbonization, a catalyst containing both Co and Co_3O_2 species– $\text{Co}_3\text{O}_4/\text{Co}$ -NPC was obtained. Melamine was used as a source of nitrogen, and after the carbonization at different temperatures, the product obtained at $800 \text{ }^\circ\text{C}$ had the optimal characteristics [92–94]. The synergistic effect of the $\text{Co}_3\text{O}_4/\text{Co}$ active species and NPC was responsible for the desired mass transport and charge transfer and the specific dual activity towards ORR and OER.

CV measurements were conducted to evaluate the ORR activity. In 0.1 M KOH solution, $\text{Co}_3\text{O}_4/\text{Co}$ -NPC had a peak at 0.738 V, which was at more positive potentials compared to Pt/C. The onset potential obtained by LSV was 0.91 V due to its value being smaller than that for Pt/C (0.987 V) and its half-wave potential being 0.806 V vs. RHE (less than the half-wave potential for Pt/C 0.8875 V). This result encourages the application of the synthesized catalyst for ORR catalysis. According to K–L plots, the average electron transfer number at the potential from 0.25 to 0.45 V was 3.9, indicating a four-electron mechanism for ORR. The chronoamperometric curves of $\text{Co}_3\text{O}_4/\text{Co}$ -NPC and Pt/C were compared to define the tolerance to methanol, where the synthesized catalyst had a negligible response after the addition of methanol and thus showed better tolerance. O_2 -saturated 0.1 M KOH at 0.5 V (vs. RHE), with a rotating speed of 1600 rpm, was used to determine the long-term stability, where, after 7 h, $\text{Co}_3\text{O}_4/\text{Co}$ -NPC had a current value at 94.5% compared to Pt/C (86.5%). Thus, the porous N-doped carbon hybrid with Co and Co_3O_4 was suggested as the promising ORR and OER agent [80].

Alginate fibers (AF) which formed an “egg-box” structure with Co^{2+} ions were used as growing sites for the coating of Co-based ZIF (Zeolitic imidazolate frameworks)-MOF (metal organic framework), and by applying the solvothermal process, the AF@ZIF-67 was obtained [95]. Synthesized material was carbonized at different temperatures, and optimal characteristics were shown by the Co-CF obtained at temperatures of $900 \text{ }^\circ\text{C}$ in an N_2 atmosphere. Due to the specific structure formed, Co and N, which were uniformly distributed on the one-dimensional CFs, were active sites and had the effect of accelerating the process of mass transfer and the transmission of electrons [96]. As ZIFs were composed of molecules with a large number of N atoms, after carbonization, the CoNC-CF material was obtained, which was shown to be an efficient catalyst for the ORR reaction. In 0.1 KOH, the half-wave potential was 0.833 V vs. RHE, and the onset potential was 0.926 V (vs. RHE) compared to 0.827 V and 0.942 V vs. RHE, respectively, for 20 wt.% Pt/C. The limiting current density was -5.56 mA^{-2} , and, compared with catalysts without N and Co active sites, the aforementioned catalyst had obvious advantages, as stated. The authors confirmed that the reduction reaction occurred through a four-electron pathway according to K–L plots. After 20,000 s, at 1600 rpm, CoNC-CF pyrolyzed at $900 \text{ }^\circ\text{C}$ had 94.8% of relative current in contrast to Pt/C, with a retention of 80.9% [95].

Compared to previously reported materials, the greatest disadvantage of this material would be its 1D structure. Despite that, the obtained material has been shown to be an excellent ORR catalyst.

The synthesis of Fe₂N/C ORR catalysts via a simple, eco-friendly route, where Fe³⁺ cations formed a novel structure of an “egg box” with alginate in the excellent yields, was described in work of Liu et al. [14]. Fe₂N nanoaerogels had outstanding ORR electrocatalytic activity, stability, and methanol tolerance in alkaline as well as in an acidic medium.

The (SA) was mixed with graphene; thus, the dispersion was obtained. The mixture was added to the FeCl₃ solution, and hydrogel was formed [63,65,97]. Upon a freeze-drying process, 3D Fe-alginate/graphene aerogels (GAs) were made, and as the size of the aerogel was only limited by the size of the container where the ion-exchange process took place, the proposed method may be a facile strategy for scaling up the production of Fe₂N/N-GAs from brown algae. After calcination at different temperatures, the material obtained at 700 °C in the NH₃ atmosphere, i.e., the optimal 3D Fe₂N/N-GAs, was formed. The 3D Fe₂N/N-GAs had a high-density N-doped amorphous carbon shell (N-AC) which encapsulated Fe₂/N NPs. This characteristic presents the great advantage of this material, considering that some Fe/N/C electrocatalysts for ORR did not have the controlled porous structure; thus, active sites were not exposed adequately, and transport properties were poor. The resulting aerogel was bimodal, as 3D mesoporous networks of about 30 nm and small mesopores of 3 nm were achieved, where the specific surface area was 465 m² g⁻¹ [14]. The molecular transport throughout the entire 3D architecture was supposed/achieved, and small mesopores were beneficial for the O₂ adsorption in the ORR [98]. The rate-determining step in the ORR, i.e., the splitting of O-O bonds as a consequence of the transfer of two electrons from active sites to adsorbed O₂, was influenced by quaternary-type and pyridine-like nitrogen, while the Fe was probably the site for O₂ adsorption.

The Fe₂N-based nanoaerogels had electrocatalytic activity for ORR in 0.1 M KOH and 1 M HClO₄ solution. In an alkaline medium, the onset potential and half-wave potentials were 1.02 V and 0.93 V, respectively, while in an acidic medium, those values were 0.82 V for the onset and 0.71 V for the half-wave potential vs. RHE. The electron transfer number was four, and the current density was -4.5 mA cm⁻². By comparing the durability of Fe₂N/N-GAs with that of Pt/C, the authors showed that the durability in acidic and alkaline media was better for Fe₂N/N-GAs. After 9 h, there was only a 10% loss of the initial current density in KOH (for Pt/C, 20%), while in HClO₄, there was a 19% loss after 10.5 h (for Pt/C, 45%). Fe₂N/N-GAs also had a good ability to resist the crossover effect; thus, there was no noticeable change in the current density after the addition of methanol [14]. This excellent catalytic activity was probably a consequence of an optimal balance of the surface area, the density of the active sites, and the electrical conductivity [99].

Yu. et al. [100] developed a simple and universal method for obtaining single-atom catalysts (SACs) with a surface area of 1551 m² g⁻¹ using Cu ion as a representative of transition metals that can form a network with alginate (i.e., “egg-box” structure). As one of the main problems for the investigation of SACs applications is the lack of a universal method for synthesis, these authors have significantly contributed to the development of SACs. In addition, they avoided physical and traditional chemical approaches which usually result in low production, complex equipment, a cumbersome process, and a high cost [101,102].

After the calcium from Ca-alginate (derived from sodium alginate) was replaced with H⁺ ions, the chemical reaction with CuCl₂ was enabled. Hydrogel consisting of Cu and alginate was dried and carbonized at 900 °C under an NH₃ atmosphere. With the aim of eliminating the metal ions, the obtained material was washed with an acidic solution. The obtained product, Cu-SAC/N, was examined for ORR activity, as well as SACs synthesized using the same procedure but with different transition metals, such as Fe-, Co-, and Mn. For catalysts obtained with Cu, in 0.1 M KOH, the onset potential was 0.90 V, and the half-wave potential was 0.80 V vs. RHE. Compared to the onset and half-wave potentials for the Pt/C catalyst (0.93 and 0.83 V, respectively), the newly synthesized material had an improved electrocatalytic activity, primarily owing to the catalytic site, which was Cu-N₄. As in the majority of experimentally obtained materials, only surface atoms acted as active sites, and the SACs have a great atom utilization efficiency. The experimentally obtained transfer

electron number was about four. After the addition of methanol, the current remained stable. The same trend was achieved by analyzing the current density after 3000 cycles of the CV, where the decrease was not more than 10%.

To summarize, a comparative table with the indicated method for obtaining the type of carbon material and the characteristics of the ORR catalysts derived from alginate is given in Table 3.

Table 3. ORR catalysts derived from alginate; characteristics, methods for obtention, and type of carbon materials.

Reference	[63]	[70]	[75]	[78]	[80]	[95]	[14]	[100]
Specific area	283 m ² g ⁻¹	485.2 m ² g ⁻¹	252 m ² g ⁻¹	222 m ² g ⁻¹	496.4 m ² g ⁻¹	/	465 m ² g ⁻¹	1551 m ² g ⁻¹
Heteroatom	N	N and S eliminated upon annealing	N	N	N	N	N	N
Dopant	/	/	Co	Co, Ni	Co	Co	Fe	Cu
Half-wave potential of catalyst/Pt/C	0.810V vs. RHE1	0.84 V vs. RHE	0.827 V vs. RHE	0.74 V vs. RHE	0.806 V vs. RHE	0.833 V vs. RHE	0.93 V vs. RHE	0.80 V vs. RHE
Optimal preparation temperature	600 °C	1000 °C	1000 °C	400 °C	800 °C	900 °C	700 °C	900 °C
Derived catalyst	N-doped porous graphitic carbon nanofibers	defective carbon fibers	3D Co/N-doped hierarchical porous carbon microspheres	carbon nanotubes nanoaerogels	Co ₃ O ₄ /Co species incorporated into the N-doped carbon matrix	carbon fiber-coated Co@N-doped porous carbonbondoped	3D Fe-alginate/graphene aerogels	single-atom catalyst
Synthesis technique	electrospun	wet spinning	electrospinning	freeze-drying	hydrothermal reaction	chemical reaction	freeze-drying	chemical reaction

3. Other Widely Used Biopolymers

Cellulose, lignin, and chitin are widely distributed polymer materials that are increasingly used as sustainable precursors for the synthesis of carbonaceous materials since they are non-toxic, biodegradable, and biocompatible [103,104].

3.1. Cellulose

Cellulose is a homopolymer consisting of glucopyranose [105]; therefore, to obtain materials with good ORR electrocatalytic activity, doping or co-doping with heteroatoms is desirable [51]. The chains of cellulose are connected in parallel, and the crystalline structure, via hydrogen and van der Waals interactions, forming microfibrils [51]. The degree of polymerization varies according to its source [106] Besides many advantages, such as the large amounts, biodegradability, low cost, etc., they also have some disadvantages; the low moisture resistance may be the most important [107].

Kim et al. used cellulose as the biomaterial for the high-value-added N-doped hierarchical porous carbon (NHPC) [108].

They developed a simple, inexpensive, and efficient process in which they mixed cotton cellulose with magnesium nitrate hexahydrate or magnesium acetate tetrahydrate and urea in different proportions. As previously reported methods included high-cost materials and low outputs, this method presents a great improvement. Upon drying, the mixture was pre-pyrolyzed at 500 °C in an Ar atmosphere. Afterwards, the obtained material was carbonized at different temperatures. The authors explained in detail the influence of the preparation parameters and contributed to the improvement of the methodology of making carbon-based ORR catalysts. Pyrolysis and carbonization were separated in order

to characterize the material after pyrolysis and to avoid the pollution of high-temperature furnaces due to a large amount of gas emission. The treatment with an acidic solution was applied after the carbonization with the aim of obtaining a final material without metal ions.

The novelty of the proposed method was that the authors used accelerated pyrolysis, where the exothermic reactions were caused by the application of nitrates, which encouraged pyrolysis at low temperatures and the rapid exfoliation of cellulose fibers. In addition, urea was used as an additional source of nitrogen but also as a reactant that supports the total exfoliation of cellulose when applied in the optimal content (Figure 4). Consequently, the sample synthesized with magnesium nitrate and urea had a highly 3D porous structure with macropores, mesopores, and abundant micropores and a specific surface area of $1173 \text{ m}^2 \text{ g}^{-1}$. Graphitic and pyridinic N, i.e., the N-C parts of the catalysts, were considered as active sites, and the high specific surface area combined with the hierarchical open pore structure contributed to the increase in the exposed active sites, thus enabling efficient mass transport and fast ion transport. According to the electrochemical measurements, including CV and LSV, the onset potential was 0.94 V, the half-wave potential was 0.83 V, and the estimated number of transferred electrons was in the range of 3.5–4 for the sample carbonized at a temperature of $1000 \text{ }^\circ\text{C}$. As the temperature of carbonization influences the doping amount and doping species of N, as the graphitization degree of the carbon, according to the stated results, the optimal temperature was $1000 \text{ }^\circ\text{C}$. The durability of the optimal material was better compared to that of the Pt/C catalyst, as the current obtained by the chronoamperometric measurements was 88% after 10 h in KOH, while for the Pt/C, it was 83% at 0.6 V vs. RHE in the O_2 -saturated KOH solution at a rotating speed of 1600 rpm. The material was methanol-tolerant, as the current had no significant changes after the addition of 2% methanol, while for the Pt/C, the current decreased [108].

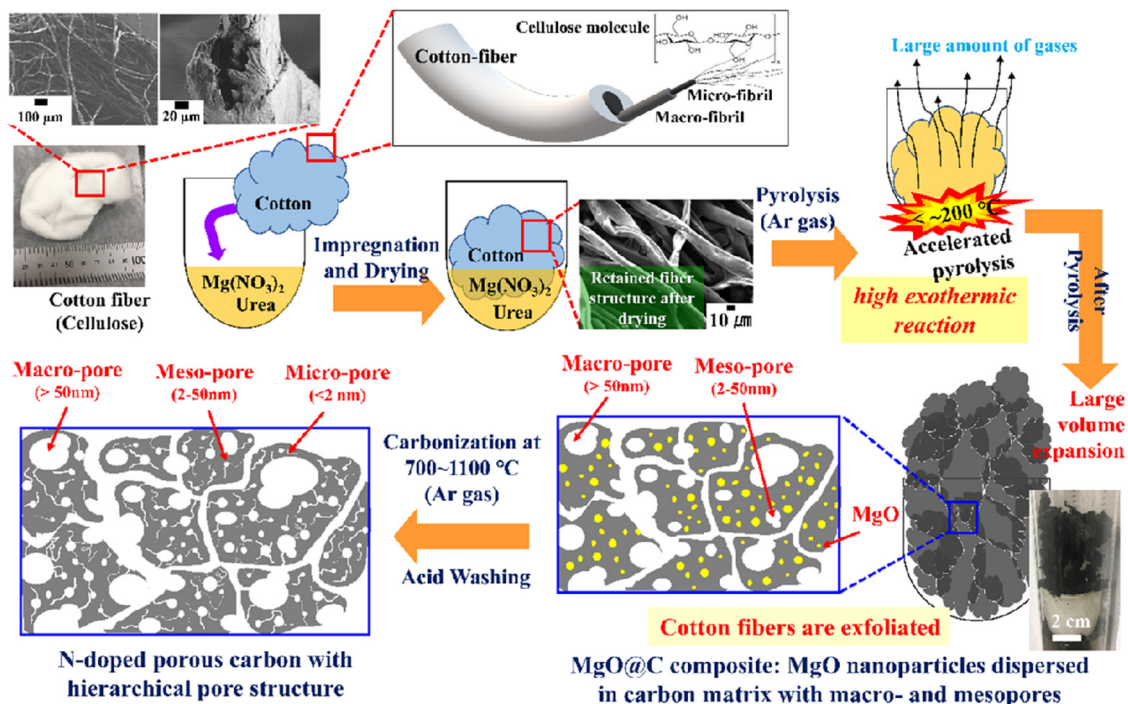


Figure 4. Schematic diagram of the preparation of N-doped porous carbon particles with a hierarchical pore structure from cellulose. Reprinted with permission from [108]. Copyright 2019 American Chemical Society.

3.2. Chitin

Chitin is, besides cellulose, the most widespread biopolymer [109,110]. It has a high content of nitrogen. Before using from the biomass, the chitin has to be extracted. This

process includes mechanical grinding, chemical demineralization, and deprotonation, techniques that may be time-demanding. In addition, the direct carbonization of chitin could not provide a defined morphology and porosity of the newly obtained material [111]. Chitosan, the deacetylated form of chitin with a different degree of deacetylation, may also be used for different purposes [110,112]. As chitosan contains about 7% of N, it presents a valuable resource of material containing carbon and nitrogen from amine and acetamide functional groups [57,103,113,114], which, upon thermal treatment, may exclude an additional step of N-doping in the synthesis process of functionalized carbons.

The specific surface area and the type of functional groups [115], both dependent on the carbonization temperature, are the main factors favoring an increase in the catalytic activity for N-doped porous carbons obtained from chitin and chitosan. The urea treatment of these materials had a great benefit for their ORR performance, since it further increased the specific surface area and enhanced the N-doping [116].

Wang et al. designed cobalt- and nitrogen-co-doped carbon material (CoNC), using a mixture of chitin and cobalt as a precursor, through a one-step pyrolysis process at 800 °C [117]. The obtained CoNC showed a specific area of 165 m² g⁻¹, and it was reported as a good material for ORR electrocatalysts in alkaline media for Al-air batteries. The onset potential was 0.86 V vs. RHE, and the high-limiting current density of 4.91 mA cm⁻² was comparable to those obtained for Pt/C 0.9 V and 5.67 mA cm⁻². The electron-transfer number was 3.73. The long-time durability was examined at 900 rpm in 0.1 M KOH saturated with O₂, and after 15,000 s, the current density was 94.82%.

3.3. Lignin

Lignin is the by-product obtained in the process of pulping. It is the constituent of grass, trees, and plants [118].

Lignin presents an amorphous aromatic polymer [58] which consists of p-hydrophenyl (H), syringyl (S), and guaiacyl (G) components, which form a three-dimensional structure. As lignin has a high content of benzene rings and phenolic functional groups, it is widely used as a precursor for the synthesis of carbon material (carbon spheres, nanofibers, nanosheets, 3D-porous carbon, carbon composites, etc.). The availability, low cost, the unique designability and controllability of the lignin structure are certainly its great advantages for its usage in different spheres [58]. The disadvantages of lignin include the fact that its usage may be a complicated procedure that disables the large-scale production. Accordingly, the development of an environmentally friendly process for the production of carbon materials from lignin is mandatory, with special attention given to the fact that the relationship between the structure of carbonized lignin and its catalytic activity is not absolutely understood yet.

The reported carbon materials derived from lignin include nitrogen-doped and nitrogen/sulfur- and nitrogen-phosphorus-co-doped catalysts [119–121]. Li et al. [122] used lignosulfonate and synthesized a robust multifunctional carbon catalyst for ORR, OER, and hydrogen evolution reaction (HER), which contained iron, nitrogen, phosphorus, and sulfur. Although different methods for carbon-doping were reported, the catalytic activity for the ORR, OER, and HER of such materials was not satisfactory. The improvement was achieved by the synthesis of the catalyst with a larger specific surface area, where active sites were exposed to the surface. The highly porous structure improved the rate of mass/electron transfer, the doping with heteroatoms upgraded the electroconductibility and charge transfer, and the FeN_x and FeP_x species had an impact on the prevention of the agglomeration of active sites and thus provided great durability. Finally, the obtained catalyst had the intrinsic activity of each active site and, consequently, great activity toward these three different reactions. The material was synthesized during the process that consisted of the preparation of lignin-Fe, and then the obtained substance was mixed with hypophosphite (inorganic molten salt template), annealed at 500 °C, and carbonized at 800 °C. After treatment with HCl solution, the material was again annealed at 800 °C and tested for catalytic activity [122]. The obtained catalyst had a specific surface area

of $782 \text{ m}^2 \text{ g}^{-1}$, which is larger than that of some reported catalysts [121]. The half-wave potential was 0.9 V, and the electron transfer number was 3.9. After injecting 3 M methanol, the current density had a negligible change, indicating a robust tolerance to methanol [122]. After 86,400 s, the current changed by 9.1%, while for the Pt/C, the change was 17.1%. Shen et al. [121] used lignin with melamine to form lignin carbon nanosheets of a surface area of $1208 \text{ m}^2 \text{ g}^{-1}$ co-doped with nitrogen and sulfur. The material may be used in an acid medium as well as in alkaline due to its better performances compared to Pt/C (a more positive half-wave potential and (nearly) current density and a high graphitic N ratio including four electron mechanisms for ORR).

4. Biomass Used for the ORR Catalysts Preparation

The carbonization of waste biomass, including adequate pre- and post-treatment processes, can be used for the preparation of ORR catalysts. Biobased N-doped carbons have been synthesized from coconut shell particles, shrimp shell, and even hair.

Due to the specificity of the structure formed by cross-linked cellulose, hemicellulose, and lignin molecules, coconut shells have a high density and low porosity; they therefore represent a good precursor material whose carbonization produces catalysts of high carbon contents and low ash residues [123]. Borghei et al. [124] developed an environmentally friendly method, without using hazardous chemicals to synthesize N/P-doped porous carbon, where, after the single-step activation of coconut shells with phosphoric acid, urea was the source of nitrogen doping. New material obtained after carbonization at $1000 \text{ }^\circ\text{C}$ with a specific surface area of $1260 \text{ m}^2 \text{ g}^{-1}$ had a comparable electrocatalytic activity with Pt/C, a better tolerance to methanol crossover, and an improved long-term durability in alkaline media.

Although it is shown that the tailoring of the pore size distribution is better achieved through physical activation [125], the authors performed the activation chemically using phosphoric acid, which led to the high-yield synthesis of carbons with a three-dimensional structure of a high porosity. The long-term stability was evaluated by chronoamperometry at 0.7 V and at 900 rpm after 50,000 s, and the results showed that the functionalization with urea improved the stability by reaching a plateau of about 75% after 13 h. The tolerance to methanol was examined, where the current intensity was the same before and after the addition of methanol, which indicated a good selectivity of the material toward the ORR. The excellent electrocatalytic activity of this material may be the result of different factors, including the contribution of a large fraction of mesopores, which enables enhanced electrolyte mass transport and the easy access of oxygen molecules to the active sites due to the 3D open pore structure, the synergic effect of N and P doping, and the large proportion of N-graphitic and N-pyridinic species. The authors suggested that the O_2 adsorption probably occurred on N-graphitic sites, while N-pyridinic sites enabled fast decomposition or an electroreduction of hydroperoxide, resulting in a fast conversion of oxygen molecules [126]. Nevertheless, the influence of the N-doping level and ORR activity still remains absolutely defined [127,128]

Jahran et al. [123] also reported the synthesis of N-doped activated carbon from coconut shells with bifunctional electrocatalytic activities towards ORR and OER, showing a good stability in alkaline electrolytes. First, they pulverized the coconut shells, soaked them overnight with 50 wt.% HNO_3 , and exposed them to a temperature of $550 \text{ }^\circ\text{C}$ under the N_2 atmosphere. After the functionalization of the material, the N-doping was accomplished with urea, and the obtained product was subsequently pyrolyzed at $900 \text{ }^\circ\text{C}$.

N-doped material had a three-dimensional structure with pores, and upon the presence of nitrogen, it had an enhanced electrocatalytic performance, a higher current density, and a more positive onset potential compared to raw material. The authors used a K–L plot to determine the number of electrons transferred in ORR, where a direct four-electron reduction pathway was obtained for N-doped activated carbon [123]. The LSV analysis of the material confirmed that the presence of nitrogen enhances the electrocatalytic activity, i.e., enables a more positive onset potential and a higher current density. The durability

of the prepared material was better compared to that of Pt/C since there was a slow decrease in the current after 1000 s in 0.1 M KOH. The authors claimed that the method was optimal for ORR catalyst synthesis, but no data for the onset and half-wave potential were presented.

Liu et al. presented a simple template-assisted method for ORR catalyst development using shrimp-shell-based carbons [129]. Shrimp waste is seafood production waste [110,130], and chitin is one of the most important parts of a shrimp shell, as it makes up as much as 40% of the shrimp mass [110,131]. Shrimp shells were ground to powder and exposed to a hydrothermal reaction such that N-doped carbon nanodots (N-CN) were formed. N-CN reacted with SiO₂ spheres under experimental conditions that were optimal for obtaining N-CN@SiO₂, which can be pyrolyzed in an N₂ atmosphere at 800 °C. At the end of the process, SiO₂ was removed, and the material with an intact three-dimensional N-doped porous carbon network was obtained. A three-modal-pore structure was noticed, with micro-, meso-, and macropores; thus, the material contained many defects in the carbon structure and, consequently, active sites for electrocatalysis predominantly consisting of pyridinic and graphitic-N [132–134]. The onset potential in 0.1 M KOH saturated with O₂ was 0.905 V, which was close to that of Pt/C. The limiting current was 5.3 mA cm⁻² at 0.6 V vs. RHE. The electron transfer number was between 3.75 and 3.95, over the potential range from 0.56 V to 0.32 V. The NPC material had no crossover effect, as the current change after the addition of 3.0 M methanol was negligible.

The authors also examined the durability, and after 20,000 s, the NPC exhibited a 12% decrease in current at a rotation speed of 1600 rpm and under an applied potential of 0.62 V, which certainly recommends the obtained material for use as an ORR catalyst [129].

Some studies suggested that carbon nanodots have high water adsorption properties, especially in an alkaline solution, due to the presence of O- and N-containing hydrophilic functional groups; thus, they could not be used as catalysts owing to the low uniformity and stability of the film made of the catalyst on the electrode [135–137]. The solution to this problem may involve the immobilization of carbon nanodots onto conductive carbon with the aim of overcoming the falling-off process [135–137]. Additionally, the low graphitization degree as a result of the low-temperature hydrothermal process, as one of the problems, may be solved by increasing the pyrolysis temperature, but agglomeration with a low surface area and an unacceptably low electrical conductivity may still be a problem [138]. Taking all of this into account, Li et al. contributed significantly to the field of efficient catalysts synthesis using biomass as a source material.

As human and animal hair can be classified as organic waste and represents the source of carbon, it can be used for the synthesis of carbon-based materials with different characteristics, including porous structures with a great surface area [53,139,140]. Chaudhari et al. [53] synthesized porous carbon material by using hair as a source of carbons and heteroatoms.

Hair consists of the α -keratin protein and thus contains nitrogen and sulfur from amino acids which are interconnected by peptide bonds [52]. Keratin is known as a protein with high content of cysteine, an amino acid rich in sulfur, making hair a good precursor material for heteroatom-doped carbon material synthesis. The specific structure of hair makes it an excellent single precursor for N- and S-doped material, consequently avoiding the usage of hazardous chemicals. Chaudhari et al. used carbonization, mild activation, and graphitization with the aim of obtaining the high-porosity material that consists of N- and S-doped carbons, which may be used as ORR catalysts. After carbonization at 250 °C in the N₂ atmosphere, the obtained char was activated at 600 °C using NaOH under a constant N₂ flow. As the graphitization was conducted at different temperatures, the temperature of 900 °C was proved to be the best for optimal ORR characteristics. The combination of heteroatom doping, a high surface area, and electrical conductivity makes the hair a promising precursor for the synthesis of ORR catalysts. The micropores and mesopores ranging from 0.5 to 4.0 nm were dominant. The specific surface area was 1813.95 m² g⁻¹. The electrochemical parameters were as follows: the onset potential was

0.949 V vs. RHE, and the reaction current was -4.92 mA cm^{-2} at 0.4 V. The electron transfer number was between 3.80 and 3.90. According to the chronoamperometry results, there was no noticeable change in the current response after 300 s of the addition of 3.0 M methanol. The durability and stability were tested at a constant potential of 0.7 V for 14 h, and after 50,000 s, the current density in 0.1 M KOH saturated with O₂ decreased by 14% at 1600 rpm.

5. Conclusions

Biopolymers contribute inestimable value towards the preparation of ORR catalysts. After appropriate treatment (mainly carbonization at an optimized temperature), these compounds give highly porous carbon material with/without dopants, making them excellent candidates for ORR catalysts. The porous carbon materials obtained from alginate are of great interest due to their low cost, wide availability, and relatively simple fabrication procedure. The inherent ability of alginate to form the “egg-box” structure after cross-linking with metal ions makes it possible to obtain materials whose electrocatalytic activity is comparable to that of Pt/C. Apart from alginate, cellulose, chitin, and lignin are excellent precursors for the preparation and production of large quantities of catalysts. As the application of Pt/C catalysts is limited by its high production costs, poor tolerance to methanol, and low durability, the limits of biopolymer applications are expanding.

Undoubtedly, natural polymers represent a wide range of compounds, which, apart from being available and affordable, have a specific structure which makes them an excellent starting compound for obtaining ORR catalysts with better durability, an improved tolerance to methanol, and better electrocatalytic properties compared to commercial ORR catalysts. Various biopolymer-derived, metal-free ORR catalysts have been studied and shown to possess excellent electrocatalytic activity, a remarkable tolerance to CO poisoning, fuel crossover effects, and a concomitant, good operational stability that is comparable to the best among non-precious metal catalysts. Porosity in biopolymer-derived carbons can ensure efficient oxygen transport and even alter the reaction mechanism, making them a viable component in PEMFCs. Despite the tremendous advancements made in the development, with heteroatom doping, a pore structure design, and surface modification, some inherent drawbacks still remain. Changes in the conductivity with higher doping levels, the lack of catalytic activity in acid media, and the difficulty of the preparation of catalysts with an exact structure and surface groups are still some of the issues that remain unresolved. The exact active site for ORR is still under debate among many researchers, many of whom turned to theoretical calculation, mainly DFT, to explore the main descriptor guiding the catalysis. Predictions of the electronic structure, active sites, reaction pathways, and intermediates provided by DFT present a part of the solution, with further research being needed to guide and connect the predictions from theoretical studies to the results from the laboratory. Biopolymer-derived, carbon-centered electrocatalysts have proved very versatile, with a great potential for improvement through doping, the pore structure, and active site design, making them an unavoidable part of the solution for many energy conversion and storage devices.

Author Contributions: J.R.: Conceptualization, Writing—Original Draft, Visualization, Writing—Review and Editing. D.T.: Visualization, Writing—Review and Editing. A.J.L.: Writing—Original Draft, Writing—Review and Editing. K.K.U.: Conceptualization, Writing—Original Draft, Supervision, Writing—Review and Editing. All authors have read and agreed to the published version of the manuscript.

Funding: This research was funded by the Ministry of Education, Science, and Technological Development, the Republic of Serbia, through a Grant Agreement with the University of Belgrade—Faculty of Pharmacy No. 451-03-68/2022-14/200161 and the University of Belgrade—Faculty of Physical Chemistry No. 451-03-68/2022-14/200146.

Data Availability Statement: Not applicable.

Conflicts of Interest: The authors declare no conflict of interest.

References

1. Dühren, S.; Betz, J.; Kolek, M.; Schmuck, R.; Winter, M.; Placke, T. Toward Green Battery Cells: Perspective on Materials and Technologies. *Small Methods* **2020**, *4*, 2000039. [[CrossRef](#)]
2. Kwak, W.-J.; Rosy, Sharon, D.; Xia, C.; Kim, H.; Johnson, L.R.; Bruce, P.G.; Nazar, L.F.; Sun, Y.-K.; Frimer, A.A.; et al. Lithium-Oxygen Batteries and Related Systems: Potential, Status, and Future. *ACS Appl. Mater. Interfaces* **2020**, *12*, 6626–6683. [[CrossRef](#)] [[PubMed](#)]
3. Wang, Y.; Chu, F.; Zeng, J.; Wang, Q.; Naren, T.; Li, Y.; Cheng, Y.; Lei, Y.; Wu, F. Single Atom Catalysts for Fuel Cells and Rechargeable Batteries: Principles, Advances, and Opportunities. *ACS Nano* **2021**, *15*, 210–239. [[CrossRef](#)]
4. Carrette, L.; Friedrich, K.A.; Stimming, U. Fuel Cells: Principles, Types, Fuels, and Applications. *ChemPhysChem* **2000**, *1*, 162–193. [[CrossRef](#)]
5. Dyer, C.K. Fuel Cells for Portable Applications. *Low-Power Electron. Des.* **2002**, *106*, 31–34. [[CrossRef](#)]
6. Hilal, M.E.; Aboulouard, A.; Akbar, A.R.; Younus, H.A.; Horzum, N.; Verpoort, F. Progress of MOF-Derived Functional Materials toward Industrialization in Solar Cells and Metal-Air Batteries. *Catalysts* **2020**, *10*, 897. [[CrossRef](#)]
7. He, Y.; Yang, X.; Li, Y.; Liu, L.; Guo, S.; Shu, C.; Liu, F.; Liu, Y.; Tan, Q.; Wu, G. Atomically Dispersed Fe-Co Dual Metal Sites as Bifunctional Oxygen Electrocatalysts for Rechargeable and Flexible Zn-Air Batteries. *ACS Catal.* **2022**, *12*, 1216–1227. [[CrossRef](#)]
8. Sun, J.; Wang, N.; Qiu, Z.; Xing, L.; Du, L. Recent Progress of Non-Noble Metal Catalysts for Oxygen Electrode in Zn-Air Batteries: A Mini Review. *Catalysts* **2022**, *12*, 843. [[CrossRef](#)]
9. Slavova, M.; Mihaylova-Dimitrova, E.; Mladenova, E.; Abrashev, B.; Burdin, B.; Vladikova, D. Zeolite Based Carbon-Free Gas Diffusion Electrodes for Secondary Metal-Air Batteries. *J. Electroanal. Sci. Eng.* **2020**, *10*, 229–234. [[CrossRef](#)]
10. Wang, J.; Huang, Z.; Liu, W.; Chang, C.; Tang, H.; Li, Z.; Chen, W.; Jia, C.; Yao, T.; Wei, S.; et al. Design of N-Coordinated Dual-Metal Sites: A Stable and Active Pt-Free Catalyst for Acidic Oxygen Reduction Reaction. *J. Am. Chem. Soc.* **2017**, *139*, 17281–17284. [[CrossRef](#)]
11. Debe, M.K. Electrocatalyst Approaches and Challenges for Automotive Fuel Cells. *Nature* **2012**, *486*, 43–51. [[CrossRef](#)] [[PubMed](#)]
12. Wu, G.; More, K.L.; Johnston, C.M.; Zelenay, P. High-Performance Electrocatalysts for Oxygen Reduction Derived from Polyaniline, Iron, and Cobalt. *Science* **2011**, *332*, 443–447. [[CrossRef](#)] [[PubMed](#)]
13. Du, L.; Zhang, G.; Liu, X.; Hassanpour, A.; Dubois, M.; Tavares, A.C.; Sun, S. Biomass-Derived Nonprecious Metal Catalysts for Oxygen Reduction Reaction: The Demand-Oriented Engineering of Active Sites and Structures. *Carbon Energy* **2020**, *2*, 561–581. [[CrossRef](#)]
14. Liu, L.; Yang, X.; Ma, N.; Liu, H.; Xia, Y.; Chen, C.; Yang, D.; Yao, X. Scalable and Cost-Effective Synthesis of Highly Efficient Fe₂N-Based Oxygen Reduction Catalyst Derived from Seaweed Biomass. *Small* **2016**, *12*, 1295–1301. [[CrossRef](#)]
15. Popadić, D.; Gavrilov, N.; Ignjatović, L.; Krajišnik, D.; Mentus, S.; Milojević-Rakić, M.; Bajuk-Bogdanović, D. How to Obtain Maximum Environmental Applicability from Natural Silicates. *Catalysts* **2022**, *12*, 519. [[CrossRef](#)]
16. Yun, S.; Hagfeldt, A.; Ma, T. Pt-Free Counter Electrode for Dye-Sensitized Solar Cells with High Efficiency. *Adv. Mater.* **2014**, *26*, 6210–6237. [[CrossRef](#)]
17. Zhou, Q.; Shi, G. Conducting Polymer-Based Catalysts. *J. Am. Chem. Soc.* **2016**, *138*, 2868–2876. [[CrossRef](#)]
18. Winther-Jensen, B.; Winther-Jensen, O.; Forsyth, M.; MacFarlane, D.R. High Rates of Oxygen Reduction over a Vapor Phase-Polymerized PEDOT Electrode. *Science* **2008**, *321*, 671–674. [[CrossRef](#)]
19. Bashyam, R.; Zelenay, P. A Class of Non-Precious Metal Composite Catalysts for Fuel Cells. *Nature* **2006**, *443*, 63–66. [[CrossRef](#)]
20. Gong, K.; Du, F.; Xia, Z.; Durstock, M.; Dai, L. Nitrogen-Doped Carbon Nanotube Arrays with High Electrocatalytic Activity for Oxygen Reduction. *Science* **2009**, *323*, 760–764. [[CrossRef](#)]
21. Choi, C.H.; Park, S.H.; Woo, S.I. Binary and Ternary Doping of Nitrogen, Boron, and Phosphorus into Carbon for Enhancing Electrochemical Oxygen Reduction Activity. *ACS Nano* **2012**, *6*, 7084–7091. [[CrossRef](#)] [[PubMed](#)]
22. Zhang, J.; Zhao, Z.; Xia, Z.; Dai, L. A Metal-Free Bifunctional Electrocatalyst for Oxygen Reduction and Oxygen Evolution Reactions. *Nat. Nanotechnol.* **2015**, *10*, 444–452. [[CrossRef](#)] [[PubMed](#)]
23. Meng, Y.; Voiry, D.; Goswami, A.; Zou, X.; Huang, X.; Chhowalla, M.; Liu, Z.; Asefa, T. N-, O-, and S-Tridoped Nanoporous Carbons as Selective Catalysts for Oxygen Reduction and Alcohol Oxidation Reactions. *J. Am. Chem. Soc.* **2014**, *136*, 13554–13557. [[CrossRef](#)] [[PubMed](#)]
24. Liu, Z.-W.; Peng, F.; Wang, H.-J.; Yu, H.; Zheng, W.-X.; Yang, J. Phosphorus-Doped Graphite Layers with High Electrocatalytic Activity for the Oxygen Reduction Reaction in an Alkaline Medium. *Angew. Chem. Int. Ed.* **2011**, *50*, 3257–3261. [[CrossRef](#)] [[PubMed](#)]
25. Yang, L.; Jiang, S.; Zhan, Y.; Zhu, L.; Chen, S.; Wang, X.; Wu, Q.; Ma, J.; Ma, Y. Boron-Doped Carbon Nanotubes as Metal-Free Electrocatalysts for the Oxygen Reduction Reaction. *Angew. Chem. Int. Ed.* **2011**, *50*, 7132–7135. [[CrossRef](#)]
26. Wang, S.; Iyyamperumal, E.; Roy, A.; Xue, Y.; Yu, D.; Dai, L. Vertically Aligned BCN Nanotubes as Efficient Metal-Free Electrocatalysts for the Oxygen Reduction Reaction: A Synergistic Effect by Co-Doping with Boron and Nitrogen. *Angew. Chem. Int. Ed.* **2011**, *50*, 11756–11760. [[CrossRef](#)]
27. Liang, H.; Wei, W.; Wu, Z.; Feng, X.; Mullen, K. Mesoporous Metal–Nitrogen-Doped Carbon Electrocatalysts for Highly Efficient Oxygen Reduction Reaction. *J. Am. Chem. Soc.* **2013**, *135*, 16002–16005. [[CrossRef](#)]

28. Ding, W.; Li, L.; Xiong, K.; Wang, Y.; Li, W.; Nie, Y.; Chen, S.; Qi, X.; Wei, Z. Shape Fixing via Salt Recrystallization: A Morphology-Controlled Approach To Convert Nanostructured Polymer to Carbon Nanomaterial as a Highly Active Catalyst for Oxygen Reduction Reaction. *J. Am. Chem. Soc.* **2015**, *137*, 5414–5420. [[CrossRef](#)]
29. Li, Q.; Cao, R.; Cho, J.; Wu, G. Nanocarbon Electrocatalysts for Oxygen Reduction in Alkaline Media for Advanced Energy Conversion and Storage. *Adv. Energy Mater.* **2014**, *4*, 1301415. [[CrossRef](#)]
30. Masa, J.; Xia, W.; Muhler, M.; Schuhmann, W. On the Role of Metals in Nitrogen-Doped Carbon Electrocatalysts for Oxygen Reduction. *Angew. Chemie-Int. Ed.* **2015**, *54*, 10102–10120. [[CrossRef](#)]
31. Yang, G.; Zhu, J.; Yuan, P.; Hu, Y.; Qu, G.; Lu, B.-A.; Xue, X.; Yin, H.; Cheng, W.; Cheng, J.; et al. Regulating Fe-spin state by atomically dispersed Mn-N in Fe-N-C catalysts with high oxygen reduction activity. *Nat. Commun.* **2021**, *12*, 1734. [[CrossRef](#)] [[PubMed](#)]
32. Wang, H.; Liu, R.; Li, Y.; Lu, X.; Wang, Q.; Zhao, S.; Yuan, K.; Cui, Z.; Li, X.; Xin, S.; et al. Durable and efficient hollow porous oxide spinel microspheres for oxygen reduction. *Joule* **2018**, *2*, 337–348. [[CrossRef](#)]
33. Brezny, A.C.; Johnson, S.I.; Raugei, S.; Mayer, J.M. Selectivity-Determining Steps in O₂ Reduction Catalyzed by Iron(tetramesitylporphyrin). *J. Am. Chem. Soc.* **2020**, *142*, 4108–4113. [[CrossRef](#)] [[PubMed](#)]
34. Ma, Q.; Jin, H.; Zhu, J.; Li, Z.; Xu, H.; Liu, B.; Zhang, Z.; Ma, J.; Mu, S. Stabilizing Fe-N-C Catalysts as Model for Oxygen Reduction Reaction. *Adv. Sci.* **2021**, *8*, 2102209. [[CrossRef](#)] [[PubMed](#)]
35. Zhao, M.; Liu, H.; Zhang, H.; Chen, W.; Sun, H.; Wang, Z.; Zhang, B.; Song, L.; Yang, Y.; Ma, C.; et al. A pH-universal ORR catalyst with single-atom iron sites derived from a double-laser MOF for superior flexible quasi-solid-state rechargeable Zn-air batteries. *Energy Environ. Sci.* **2021**, *14*, 6455–6463. [[CrossRef](#)]
36. Rupar, J.; Bajuk-Bogdanović, D.; Milojević-Rakić, M.; Krstić, J.; Upadhyay, K.; Gavrilov, N.; Janošević Ležaić, A. Tailored porosity development in carbons via Zn²⁺ monodispersion: Fitting supercapacitors. *Micropor. Mesopor. Mat.* **2022**, *335*, 111790. [[CrossRef](#)]
37. Zhou, H.; Zhang, J.; Amiin, I.S.; Zhan, C.; Liu, X.; Tu, W.; Pan, M.; Mu, S. Transforming Waste Biomass with an Intrinsically Porous Network Structure into Porous Nitrogen-Doped Graphene for Highly Efficient Oxygen Reduction. *Phys. Chem. Chem. Phys.* **2016**, *18*, 10392–10399. [[CrossRef](#)]
38. Huang, Y.; Wu, D.; Cao, D.; Cheng, D. Facile Preparation of Biomass-Derived Bifunctional Electrocatalysts for Oxygen Reduction and Evolution Reactions. *Int. J. Hydrog. Energy* **2018**, *43*, 8611–8622. [[CrossRef](#)]
39. Calvo-Muñoz, E.M.; García-Mateos, F.J.; Rosas, J.M.; Rodríguez-Mirasol, J.; Cordero, T. Biomass Waste Carbon Materials as Adsorbents for CO₂ Capture under Post-Combustion Conditions. *Front. Mater.* **2016**, *3*, 23. [[CrossRef](#)]
40. Xu, X.; Yuan, T.; Zhoy, Y.; Li, Y.; Li, Y.; Lu, J.; Tian, X.; Wang, D.; Wang, J. Facile synthesis of boron and nitrogen-doped graphene as efficient electrocatalyst for the oxygen reduction reaction in alkaline media. *Int. Hydrog. Energy* **2014**, *39*, 16043–16052. [[CrossRef](#)]
41. Huang, Z.-H.; Liu, T.-Y.; Song, Y.; Li, Y.; Liu, X.-X. Balancing the electrical double layer capacitance and pseudocapacitance of heteroatom doped carbon. *Nanoscale* **2017**, *35*, 13119–13127. [[CrossRef](#)] [[PubMed](#)]
42. Badosz, T.J. Porous Carbons as Oxygen Reduction Electrocatalysts. In *Porous Materials*; Springer: Berlin/Heidelberg, Germany, 2021; pp. 41–77.
43. Wu, J.; Ma, L.; Yadav, R.; Yang, Y.; Zhang, X.; Vajtai, R.; Lou, J.; Ajayan, P.M. Nitrogen-Doped Graphene with Pyridinic Dominance as a Highly Active and Stable Electrocatalyst for Oxygen Reduction. *ACS Appl. Mater. Interfaces* **2015**, *7*, 14763–14769. [[CrossRef](#)]
44. Yuan, S.; Cui, L.-L.; Dou, Z.; Ge, X.; He, X.; Zhang, W.; Asefa, T. Nonprecious Bimetallic Sites Coordinated on N-Doped Carbons with Efficient and Durable Catalytic Activity for Oxygen Reduction. *Small* **2020**, *16*, 2000742. [[CrossRef](#)]
45. Zheng, Y.; Song, H.; Chen, S.; Yu, X.; Zhu, J.; Xu, J.; Zhang, K.A.I.; Zhang, C.; Liu, T. Metal-Free Multi-Heteroatom-Doped Carbon Bifunctional Electrocatalysts Derived from a Covalent Triazine Polymer. *Small* **2020**, *16*, 2004342. [[CrossRef](#)] [[PubMed](#)]
46. Zhang, G.; Wei, Q.; Yang, X.; Tavares, A.C.; Sun, S. RRDE experiments on noble-metal and noble-metal-free catalysts: Impact of loading on the activity and selectivity of oxygen reduction reaction in alkaline solution. *Appl. Catal. B Environ.* **2017**, *206*, 115–126. [[CrossRef](#)]
47. Bouleau, L.; Pérez-Rodríguez, S.; Quílez-Bermejo, J.; Izquierdo, M.; Xu, F.; Fierro, V.; Celzard, A. Best practices for ORR performance evaluation of metal-free porous carbon electrocatalysts. *Carbon* **2022**, *189*, 349–361. [[CrossRef](#)]
48. Gabe, A.; Ruiz-Rosas, R.; Gonzales-Gaitan, C.; Morallon, E.; Cazorla-Amoros, D. Modeling of oxygen reduction reaction in porous carbon reaction in porous carbon materials in alkaline medium. Effect of microporosity. *J. Power Sources* **2019**, *412*, 451–464. [[CrossRef](#)]
49. Ye, Y.; Duan, W.; Yi, X.; Lei, Z.; Li, G.; Feng, C. Biogenic precursor to size-controlled synthesis of Fe₂P nanoparticles in heteroatom-doped graphene-like carbons and their electrocatalytic reduction of oxygen. *J. Power Sources* **2019**, *435*, 226770. [[CrossRef](#)]
50. Li, Y.; Zhang, H.; Liu, P.; Wang, Y.; Yang, H.; Li, Y.; Zhao, H. Self-supported bimodal-pore structured nitrogen-doped carbon fiber electrocatalyst for oxygen reduction reaction. *Electrochem. Commun.* **2015**, *51*, 6–10. [[CrossRef](#)]
51. Borghei, M.; Lehtonen, J.; Liu, L.; Rojas, O.J. Advanced Biomass-Derived Electrocatalysts for the Oxygen Reduction Reaction. *Adv. Mater.* **2017**, *30*, 1703691. [[CrossRef](#)]
52. Clay, R.C.; Cook, K.; Routh, J.I. Studies in the composition of human hair. *J. Am. Chem. Soc.* **1940**, *62*, 2709. [[CrossRef](#)]
53. Chaudhari, K.N.; Song, M.Y.; Yu, J.S. Transforming Hair into Heteroatom-Doped Carbon with High Surface Area. *Small* **2014**, *10*, 2625–2636. [[CrossRef](#)] [[PubMed](#)]

54. Ezeoha, S.L.; Enzenwanne, J.N. Production of Biodegradable Plastic Packaging Film from Cassava Starch. *IOSR J. Eng.* **2013**, *3*, 14–20. [[CrossRef](#)]
55. Baranwal, J.; Barse, B.; Fais, A.; Delogu, G.L.; Kumar, A. Biopolymer: A Sustainable Material for Food and Medical Applications. *Polymers* **2022**, *14*, 983. [[CrossRef](#)] [[PubMed](#)]
56. Berg, J.M.; Tymoczko, J.L.; Stryer, L. *Biochemistry*, 5th ed.; W.H. Freeman and Company: New York, NY, USA, 2002.
57. Khan, A.; Goepel, M.; Colmenares, J.C.; Gläser, R. Chitosan-Based N-Doped Carbon Materials for Electrocatalytic and Photocatalytic Applications. *ACS Sustain. Chem. Eng.* **2020**, *8*, 4708–4727. [[CrossRef](#)]
58. Wang, H.; Fu, F.; Huang, M.; Feng, Y.; Han, D.; Xi, Y.; Xiong, W.; Yang, D.; Niu, L. Lignin-Based Materials for Electrochemical Energy Storage Devices. *Nano Mater. Sci.* **2022**, *in press*. [[CrossRef](#)]
59. Wittmar, A.S.M.; Ropertz, M.; Braun, M.; Hagemann, U.; Andronescu, C.; Ulbricht, M. Preparation of N-Doped Carbon Materials from Cellulose:Chitosan Blends and Their Potential Application in Electrocatalytic Oxygen Reduction. *Polym. Bull.* **2022**, 1–19. [[CrossRef](#)]
60. Li, Y.; Liu, X.; Wang, J.; Yang, L.; Chen, X.; Wang, X.; Zhang, P. Marine Algae-Derived Porous Carbons as Robust Electrocatalysts for ORR. *Catalysts* **2019**, *9*, 730. [[CrossRef](#)]
61. Hao, Y.; Zhang, X.; Yang, Q.; Chen, K.; Guo, J.; Zhou, D.; Feng, L.; Slanina, Z. Highly Porous Defective Carbons Derived from Seaweed Biomass as Efficient Electrocatalysts for Oxygen Reduction in Both Alkaline and Acidic Media. *Carbon N. Y.* **2018**, *137*, 93–103. [[CrossRef](#)]
62. Udayakumar, G.P.; Muthusamy, S.; Selvaganesh, B.; Sivarajasekar, N.; Rambabu, K.; Sivamani, S.; Sivakumar, N.; Maran, J.P.; Hosseini-Bandegharaei, A. Ecofriendly Biopolymers and Composites: Preparation and Their Applications in Water-Treatment. *Biotechnol. Adv.* **2021**, *52*, 107815. [[CrossRef](#)]
63. Li, D.; Lv, C.; Liu, L.; Xia, Y.; She, X.; Guo, S.; Yang, D. Egg-Box Structure in Cobalt Alginate: A New Approach to Multifunctional Hierarchical Mesoporous N-Doped Carbon Nanofibers for Efficient Catalysis and Energy Storage. *ACS Cent. Sci.* **2015**, *1*, 261–269. [[CrossRef](#)]
64. Wu, X.L.; Chen, L.L.; Xin, S.; Yin, Y.X.; Guo, Y.G.; Kong, Q.S.; Xia, Y.Z. Preparation and Li Storage Properties of Hierarchical Porous Carbon Fibers Derived from Alginic Acid. *ChemSusChem* **2010**, *3*, 703–707. [[CrossRef](#)] [[PubMed](#)]
65. Li, D.; Yang, D.; Zhu, X.; Jing, D.; Xia, Y.; Ji, Q.; Cai, R.; Li, H.; Che, Y. Simple Pyrolysis of Cobalt Alginate Fibres into Co₃O₄/C Nano/Microstructures for a High-Performance Lithium Ion Battery Anode. *J. Mater. Chem. A* **2014**, *2*, 18761–18766. [[CrossRef](#)]
66. Puscaselu, R.G.; Lobiuc, A.; Dimian, M.; Covasa, M. Alginate: From Food Industry to Biomedical Applications and Management of Metabolic Disorders. *Polymers* **2020**, *12*, 2417. [[CrossRef](#)] [[PubMed](#)]
67. Fourest, E.; Volesky, B. Alginate Properties and Heavy Metal Biosorption by Marine Algae. *Appl. Biochem. Biotechnol.—Part A Enzym. Eng. Biotechnol.* **1997**, *67*, 215–226. [[CrossRef](#)]
68. Braccini, I.; Pérez, S. Molecular Basis of Ca²⁺-Induced Gelation in Alginates and Pectins: The Egg-Box Model Revisited. *Biomacromolecules* **2001**, *2*, 1089–1096. [[CrossRef](#)] [[PubMed](#)]
69. Li, P.; Jin, Z.; Qian, Y.; Fang, Z.; Xiao, D.; Yu, G. Supramolecular Confinement of Single Cu Atoms in Hydrogel Frameworks for Oxygen Reduction Electrocatalysis with High Atom Utilization. *Mater. Today* **2020**, *35*, 78–86. [[CrossRef](#)]
70. Zhao, X.; Yu, X.; Xin, S.; Chen, S.; Bao, C.; Xu, W.; Xue, J.; Hui, B.; Zhang, J.; She, X.; et al. Enhanced Oxygen Reduction Reaction for Zn-Air Battery at Defective Carbon Fibers Derived from Seaweed Polysaccharide. *Appl. Catal. B Environ.* **2022**, *301*, 120785. [[CrossRef](#)]
71. Wei, C.; Sun, Y.; Scherer, G.G.; Fisher, A.C.; Sherburne, M.; Ager, J.W.; Xu, Z.J. Surface Composition Dependent Ligand Effect in Tuning the Activity of Nickel-Copper Bimetallic Electrocatalysts toward Hydrogen Evolution in Alkaline. *J. Am. Chem. Soc.* **2020**, *142*, 7765–7775. [[CrossRef](#)]
72. Song, Q.; Li, J.; Wang, S.; Liu, J.; Liu, X.; Pang, L.; Li, H.; Liu, H. Enhanced Electrocatalytic Performance through Body Enrichment of Co-Based Bimetallic Nanoparticles In Situ Embedded Porous N-Doped Carbon Spheres. *Small* **2019**, *15*, 1–9. [[CrossRef](#)]
73. Mun, Y.; Lee, S.; Kim, K.; Kim, S.; Lee, S.; Han, J.W.; Lee, J. Versatile Strategy for Tuning ORR Activity of a Single Fe-N₄ Site by Controlling Electron-Withdrawing/Donating Properties of a Carbon Plane. *J. Am. Chem. Soc.* **2019**, *141*, 6254–6262. [[CrossRef](#)]
74. Xing, X.; Liu, R.; Anjass, M.; Cao, K.; Kaiser, U.; Zhang, G.; Streb, C. Bimetallic Manganese-Vanadium Functionalized N,S-Doped Carbon Nanotubes as Efficient Oxygen Evolution and Oxygen Reduction Electrocatalysts. *Appl. Catal. B Environ.* **2020**, *277*, 119195. [[CrossRef](#)]
75. Shu, J.; Niu, Q.; Wang, N.; Nie, J.; Ma, G. Alginate Derived Co/N Doped Hierarchical Porous Carbon Microspheres for Efficient Oxygen Reduction Reaction. *Appl. Surf. Sci.* **2019**, *485*, 520–528. [[CrossRef](#)]
76. Wang, Y.; Tao, L.; Xiao, Z.; Chen, R.; Jiang, Z.; Wang, S. 3D Carbon Electrocatalysts In Situ Constructed by Defect-Rich Nanosheets and Polyhedrons from NaCl-Sealed Zeolitic Imidazolate Frameworks. *Adv. Funct. Mater.* **2018**, *28*, 1705356. [[CrossRef](#)]
77. Zhang, Y.; Lin, Y.; Jiang, H.; Wu, C.; Liu, H.; Wang, C.; Chen, S.; Duan, T.; Song, L. Well-Defined Cobalt Catalyst with N-doped Carbon Layers Enwrapping: The Correlation between Surface Atomic Structure and Electrocatalytic Property. *Small* **2017**, *14*, 1702074. [[CrossRef](#)] [[PubMed](#)]
78. Ma, N.; Jia, Y.; Yang, X.; She, X.; Zhang, L.; Peng, Z.; Yao, X.; Yang, D. Seaweed Biomass Derived (Ni,Co)/CNT Nanoaerogels: Efficient Bifunctional Electrocatalysts for Oxygen Evolution and Reduction Reactions. *J. Mater. Chem. A* **2016**, *4*, 6376–6384. [[CrossRef](#)]

79. Zhao, W.; Yuan, P.; She, X.; Xia, Y.; Komarneni, S.; Xi, K.; Che, Y.; Yao, X.; Yang, D. Sustainable Seaweed-Based One-Dimensional (1D) Nanofibers as High-Performance Electrocatalysts for Fuel Cells. *J. Mater. Chem. A* **2015**, *3*, 14188–14194. [[CrossRef](#)]
80. Zhan, T.; Lu, S.; Liu, X.; Teng, H.; Hou, W. Alginate Derived $\text{Co}_3\text{O}_4/\text{Co}$ Nanoparticles Decorated in N-Doped Porous Carbon as an Efficient Bifunctional Catalyst for Oxygen Evolution and Reduction Reactions. *Electrochim. Acta* **2018**, *265*, 681–689. [[CrossRef](#)]
81. Zhang, C.; Antonietti, M.; Fellingner, T.P. Blood Ties: Co_3O_4 Decorated Blood Derived Carbon as a Superior Bifunctional Electrocatalyst. *Adv. Funct. Mater.* **2014**, *24*, 7655–7665. [[CrossRef](#)]
82. Wan, L.; Lin, C.; Huang, D.; Zhang, F.; Wang, M.; Jin, J. A Comparative Study of Composition and Morphology Effect of Ni $\text{XCo}_{1-x}(\text{OH})_2$ on Oxygen Evolution/Reduction Reaction. *ACS Appl. Mater. Interfaces* **2014**, *6*, 10172–10180. [[CrossRef](#)]
83. Wang, D.; Chen, X.; Evans, D.G.; Yang, W. Well-Dispersed $\text{Co}_3\text{O}_4/\text{Co}_2\text{MnO}_4$ Nanocomposites as a Synergistic Bifunctional Catalyst for Oxygen Reduction and Oxygen Evolution Reactions. *Nanoscale* **2013**, *5*, 5312–5315. [[CrossRef](#)]
84. Song, F.; Hu, X. Ultrathin Cobalt-Manganese Layered Double Hydroxide Is an Efficient Oxygen Evolution Catalyst. *J. Am. Chem. Soc.* **2014**, *136*, 16481–16484. [[CrossRef](#)] [[PubMed](#)]
85. Ryu, W.H.; Yoon, T.H.; Song, S.H.; Jeon, S.; Park, Y.J.; Kim, I.D. Bifunctional Composite Catalysts Using Co_3O_4 Nanofibers Immobilized on Nonoxidized Graphene Nanoflakes for High-Capacity and Long-Cycle Li- O_2 Batteries. *Nano Lett.* **2013**, *13*, 4190–4197. [[CrossRef](#)] [[PubMed](#)]
86. Navalon, S.; Dhakshinamoorthy, A.; Alvaro, M.; Garcia, H. Carbocatalysis by Graphene-Based Materials. *Chem. Rev.* **2014**, *114*, 6179–6212. [[CrossRef](#)] [[PubMed](#)]
87. Li, W.; Zhang, F.; Dou, Y.; Wu, Z.; Liu, H.; Qian, X.; Gu, D.; Xia, Y.; Tu, B.; Zhao, D. A Self-Template Strategy for the Synthesis of Mesoporous Carbon Nanofibers as Advanced Supercapacitor Electrodes. *Adv. Energy Mater.* **2011**, *1*, 382–386. [[CrossRef](#)]
88. You, B.; Yin, P.; Zhang, J.; He, D.; Chen, G.; Kang, F.; Wang, H.; Deng, Z.; Li, Y. Hydrogel-Derived Non-Precious Electrocatalysts for Efficient Oxygen Reduction. *Sci. Rep.* **2015**, *5*, 11739. [[CrossRef](#)] [[PubMed](#)]
89. You, B.; Kang, F.; Yin, P.; Zhang, Q. Hydrogel-Derived Heteroatom-Doped Porous Carbon Networks for Supercapacitor and Electrocatalytic Oxygen Reduction. *Carbon N. Y.* **2016**, *103*, 9–15. [[CrossRef](#)]
90. Li, Y.; Zhou, W.; Wang, H.; Xie, L.; Liang, Y.; Wei, F.; Idrobo, J.C.; Pennycook, S.J.; Dai, H. An Oxygen Reduction Electrocatalyst Based on Carbon Nanotube-Graphene Complexes. *Nat. Nanotechnol.* **2012**, *7*, 394–400. [[CrossRef](#)]
91. Zhao, Z.; Wu, H.; He, H.; Xu, X.; Jin, Y. A High-Performance Binary Ni-Co Hydroxide-Based Water Oxidation Electrode with Three-Dimensional Coaxial Nanotube Array Structure. *Adv. Funct. Mater.* **2014**, *24*, 4698–4705. [[CrossRef](#)]
92. He, W.; Jiang, C.; Wang, J.; Lu, L. High-Rate Oxygen Electroreduction over Graphitic-N Species Exposed on 3D Hierarchically Porous Nitrogen-Doped Carbons. *Angew. Chemie—Int. Ed.* **2014**, *53*, 9503–9507. [[CrossRef](#)]
93. Shibuya, R.; Kondo, T.; Nakamura, J. Active Sites of Nitrogen-Doped Carbon Materials for Oxygen Reduction Reaction Clarified Using Model Catalysts. *Carbon-Based Met. Catal. Des. Appl.* **2016**, *351*, 361–365. [[CrossRef](#)]
94. Wu, G.; Hu, Y.; Liu, Y.; Zhao, J.; Chen, X.; Whoehling, V.; Plesse, C.; Nguyen, G.T.M.; Vidal, F.; Chen, W. Graphitic Carbon Nitride Nanosheet Electrode-Based High-Performance Ionic Actuator. *Nat. Commun.* **2015**, *6*, 7258. [[CrossRef](#)]
95. Jia, N.; Li, D.; Huang, G.; Sun, J.; Lu, P.; Wan, L.; Hui, B.; She, X.; Zhao, X. Carbon Fibers-Coated Co@N-Doped Porous Carbon Derived from ZIF-67/Alginate Fibers for Efficient Oxygen Reduction Reaction. *J. Photonics Energy* **2020**, *10*, 023507. [[CrossRef](#)]
96. Guo, J.; Shu, J.; Nie, J.; Ma, G. Fe/Ni Bimetal and Nitrogen Co-Doped Porous Carbon Fibers as Electrocatalysts for Oxygen Reduction Reaction. *J. Colloid Interface Sci.* **2020**, *560*, 330–337. [[CrossRef](#)] [[PubMed](#)]
97. Lv, C.; Yang, X.; Umar, A.; Xia, Y.; Jia, Y.; Shang, L.; Zhang, T.; Yang, D. Architecture-Controlled Synthesis of MxO_y ($\text{M} = \text{Ni}, \text{Fe}, \text{Cu}$) Microfibres from Seaweed Biomass for High-Performance Lithium Ion Battery Anodes. *J. Mater. Chem. A* **2015**, *3*, 22708–22715. [[CrossRef](#)]
98. Xiao, M.; Zhu, J.; Feng, L.; Liu, C.; Xing, W. Meso/Macroporous Nitrogen-Doped Carbon Architectures with Iron Carbide Encapsulated in Graphitic Layers as an Efficient and Robust Catalyst for the Oxygen Reduction Reaction in Both Acidic and Alkaline Solutions. *Adv. Mater.* **2015**, *27*, 2521–2527. [[CrossRef](#)]
99. Liang, J.; Zhou, R.F.; Chen, X.M.; Tang, Y.H.; Qiao, S.Z. Fe-N decorated hybrids of CNTs grown on hierarchically porous carbon for high-performance oxygen reduction. *Adv. Mater.* **2014**, *26*, 6074–6079. [[CrossRef](#)]
100. Yu, L.Q.; Xia, W.J.; Ma, W.J.; Wen, T.E.; Chen, S.L.; Jin, F.; Huang, B.C.; Jin, R.C. Universal Method to Fabricate Transition Metal Single-Atom-Anchored Carbon with Excellent Oxygen Reduction Reaction Activity. *ACS Appl. Mater. Interfaces* **2021**, *13*, 13534–13540. [[CrossRef](#)]
101. Kaden, W.E.; Wu, T.; Kunkel, W.A.; Anderson, S.L. Electronic structure controls reactivity of size-selected Pd clusters adsorbed on TiO_2 surfaces. *Science* **2009**, *326*, 826–829. [[CrossRef](#)]
102. Liu, P.; Zhao, Y.; Qin, R.; Mo, S.; Chen, G.; Gu, L.; Chevrier, D.M.; Zhang, P.; Qing, G.; Zang, D.; et al. Photochemical route for synthesizing atomically dispersed palladium catalysts. *Science* **2016**, *352*, 797–801. [[CrossRef](#)]
103. Varma, R.S. Biomass-Derived Renewable Carbonaceous Materials for Sustainable Chemical and Environmental Applications. *ACS Sustain. Chem. Eng.* **2019**, *7*, 6458–6470. [[CrossRef](#)]
104. Zahedifar, M.; Es-Haghi, A.; Zhiani, R.; Sadeghzadeh, S.M. Synthesis of Benzimidazolones by Immobilized Gold Nanoparticles on Chitosan Extracted from Shrimp Shells Supported on Fibrous Phosphosilicate. *RSC Adv.* **2019**, *9*, 6494–6501. [[CrossRef](#)] [[PubMed](#)]
105. Klemm, D.; Philipp, B.; Heinze, T.; Heinze, U.; Wagenknecht, W. General Considerations on Structure and Reactivity of Cellulose: Section 2.3–2.3.7. In *Comprehensive Cellulose Chemistry*; Wiley-VCH Verlag GmbH: New York, NY, USA, 1998; Volume 1, pp. 83–129. ISBN 3527294139.

106. Abe, M.M.; Ribeiro Martins, J.; Bertolino Sanvezzo, P.; Macedo, J.V.; Branciforti, M.C.; Halley, P.; Botaro, V.R.; Brienzo, M. Advantages and Disadvantages of Bioplastics Production from Starch and Lignocellulosic Components. *Polymers* **2021**, *13*, 2484. [[CrossRef](#)] [[PubMed](#)]
107. Sahu, P.; Gupta, M.K. Water absorption behavior of cellulosic fibres polymer composites: A review on its effects and remedies. *J. Ind. Text.* **2020**, *51*, 7480S–7512S. [[CrossRef](#)]
108. Kim, C.; Zhu, C.; Aoki, Y.; Habazaki, H. Exothermally Efficient Exfoliation of Biomass Cellulose to Value-Added N-Doped Hierarchical Porous Carbon for Oxygen Reduction Electrocatalyst. *Ind. Eng. Chem. Res.* **2019**, *58*, 3047–3059. [[CrossRef](#)]
109. Kurita, K. Chitin and Chitosan: Functional Biopolymers from Marine Crustaceans. *Mar. Biotechnol.* **2006**, *8*, 203–226. [[CrossRef](#)]
110. Bradic, B. Isolation of Chitin from Marine Biomass Using Eutectic Solvents and Studies of N-Deacetylation Kinetics to Chitosan. Doctoral Dissertation, Univerza v Mariboru, Bojana Bradić, Slovenia, 2020.
111. De, S.; Acharya, S.; Sahoo, S.; Nayak, G.C. Chapter 12- Present status of biomass-derived carbon-based composites for supercapacitor application. In *Nanostructured, Functional, and Flexible Materials for Energy Conversion and Storage Systems*; Pandikumar, A., Rameshkumar, P., Eds.; Elsevier: Amsterdam, The Netherlands, 2020; pp. 373–415. [[CrossRef](#)]
112. Anitha, A.; Sowmya, S.; Kumar, P.T.S.; Deepthi, S.; Chennazhi, K.P.; Ehrlich, H.; Tsurkan, M.; Jayakumar, R. Chitin and Chitosan in Selected Biomedical Applications. *Prog. Polym. Sci.* **2014**, *39*, 1644–1667. [[CrossRef](#)]
113. Verma, S.; Nadagouda, M.N.; Varma, R.S. Porous Nitrogen-Enriched Carbonaceous Material from Marine Waste: Chitosan-Derived Carbon Nitride Catalyst for Aerial Oxidation of 5-Hydroxymethylfurfural (HMF) to 2,5-Furandicarboxylic Acid. *Sci. Rep.* **2017**, *7*, 13596. [[CrossRef](#)]
114. Primo, A.; Atienzar, P.; Sanchez, E.; Delgado, J.M.; García, H. From Biomass Wastes to Large-Area, High-Quality, N-Doped Graphene: Catalyst-Free Carbonization of Chitosan Coatings on Arbitrary Substrates. *Chem. Commun.* **2012**, *48*, 9254–9256. [[CrossRef](#)]
115. Skorupska, M.; Ilnicka, A.; Lukaszewicz, J.P. Successful Manufacturing Protocols of N-Rich Carbon Electrodes Ensuring High ORR Activity: A Review. *Processes* **2022**, *10*, 643. [[CrossRef](#)]
116. Ilnicka, A.; Lukaszewicz, J.P.; Shimano, K.; Yuasa, M. Urea treatment of nitrogen-doped carbon leads to enhanced performance for the oxygen reduction reaction. *J. Mater. Res.* **2018**, *33*, 1612–1624. [[CrossRef](#)]
117. Wang, M.; Ma, J.; Yang, H.; Lu, G.; Yang, S.; Chang, Z. Nitrogen and Cobalt Co-Doped Carbon Materials Derived from Biomass Chitin as High-Performance Electrocatalyst for Aluminium-Air Batteries. *Catalysts* **2019**, *9*, 954. [[CrossRef](#)]
118. Hatakeyama, H.; Hatakeyama, T. Lignin Structure, Properties, and Applications. *Adv. Polym. Sci.* **2009**, *232*, 1–63. [[CrossRef](#)]
119. Zheng, Y.; Chen, S.; Zhang, K.A.I.; Guan, J.; Yu, X.; Peng, W.; Song, H.; Zhu, J.; Xu, J.; Fan, X.; et al. Template-Free Construction of Hollow Mesoporous Carbon Spheres from a Covalent Triazine Framework for Enhanced Oxygen Electroreduction. *J. Colloid Interface Sci.* **2022**, *608*, 3168–3177. [[CrossRef](#)]
120. Li, W.; Zhang, H.; Zhang, K.; Hu, W.; Cheng, Z.; Chen, H.; Feng, X.; Peng, T.; Kou, Z. Monodispersed Ruthenium Nanoparticles Interfacially Bonded with Defective Nitrogen-and-Phosphorus-Doped Carbon Nanosheets Enable PH-Universal Hydrogen Evolution Reaction. *Appl. Catal. B Environ.* **2022**, *306*, 121095. [[CrossRef](#)]
121. Shen, Y.; Peng, F.; Cao, Y.; Zuo, J.; Wang, H.; Yu, H. Preparation of Nitrogen and Sulfur Co-Doped Ultrathin Graphitic Carbon via Annealing Bagasse Lignin as Potential Electrocatalyst towards Oxygen Reduction Reaction in Alkaline and Acid Media. *J. Energy Chem.* **2019**, *34*, 33–42. [[CrossRef](#)]
122. Li, P.; Wang, H.; Fan, W.; Huang, M.; Shi, J.; Shi, Z.; Liu, S. Salt Assisted Fabrication of Lignin-Derived Fe, N, P, S Codoped Porous Carbon as Trifunctional Catalyst for Zn-Air Batteries and Water-Splitting Devices. *Chem. Eng. J.* **2021**, *421*, 129704. [[CrossRef](#)]
123. Jahan, M.; Feni, F. Environmentally Friendly Bifunctional Catalyst for ORR and OER from Coconut Shell Particles. *Adv. Mater. Phys. Chem.* **2022**, *12*, 106–123. [[CrossRef](#)]
124. Borghei, M.; Laocharoen, N.; Kibena-Pöldsepp, E.; Johansson, L.S.; Campbell, J.; Kauppinen, E.; Tammeveski, K.; Rojas, O.J. Porous N,P-Doped Carbon from Coconut Shells with High Electrocatalytic Activity for Oxygen Reduction: Alternative to Pt-C for Alkaline Fuel Cells. *Appl. Catal. B Environ.* **2017**, *204*, 394–402. [[CrossRef](#)]
125. Prauchner, M.J.; Rodríguez-Reinoso, F. Chemical versus Physical Activation of Coconut Shell: A Comparative Study. *Microporous Mesoporous Mater.* **2012**, *152*, 163–171. [[CrossRef](#)]
126. Borghei, M. Novel carbon nanomaterials for the direct methanol fuel cell electrodes. Doctoral Dissertation, Aalto University, School of Science, Department of Applied Physics, NanoMaterials Group, Maryam Borghei, Espoo, Finland, 2015.
127. Nagaiah, T.C.; Kundu, S.; Bron, M.; Muhler, M.; Schuhmann, W. Nitrogen-doped carbon nanotubes as a cathode catalyst for the oxygen reduction reaction in alkaline medium. *Electrochem. Commun.* **2010**, *12*, 338–341. [[CrossRef](#)]
128. Oh, H.-S.; Oh, J.-G.; Hee Lee, W.; Kim, H.-J.; Kim, H. The influence of the structural properties of carbon on the oxygen reduction reaction of nitrogen modified carbon based catalysts. *Int. J. Hydrog. Energy* **2011**, *36*, 8181–8186. [[CrossRef](#)]
129. Liu, R.; Zhang, H.; Liu, S.; Zhang, X.; Wu, T.; Ge, X.; Zang, Y.; Zhao, H.; Wang, G. Shrimp-Shell Derived Carbon Nanodots as Carbon and Nitrogen Sources to Fabricate Three-Dimensional N-Doped Porous Carbon Electrocatalysts for the Oxygen Reduction Reaction. *Phys. Chem. Chem. Phys.* **2016**, *18*, 4095–4101. [[CrossRef](#)] [[PubMed](#)]
130. Yan, N.; Chen, X. Don't Waste Seafood Waste: Turning Cast-off Shells into Nitrogen-Rich Chemicals Would Benefit Economies and the Environment. *Nature* **2015**, *524*, 155–157. [[CrossRef](#)] [[PubMed](#)]
131. Tokatl, K.; Demirdöven, A. Optimization of Chitin and Chitosan Production from Shrimp Wastes and Characterization. *J. Food Process. Preserv.* **2017**, *42*, e13494. [[CrossRef](#)]

132. Tuci, G.; Zafferoni, C.; Rossin, A.; Milella, A.; Luconi, L.; Innocenti, M.; Truong Phuoc, L.; Duong-Viet, C.; Pham-Huu, C.; Giambastiani, G. Chemically Functionalized Carbon Nanotubes with Pyridine Groups as Easily Tunable N-Decorated Nanomaterials for the Oxygen Reduction Reaction in Alkaline Medium. *Chem. Mater.* **2014**, *26*, 3460–3470. [[CrossRef](#)]
133. Xie, J.; Zhang, H.; Li, S.; Wang, R.; Sun, X.; Zhou, M.; Zhou, J.; Wen, X.; Lou, D.; Xie, Y. Defect-Rich MoS₂ Ultrathin Nanosheets with Additional Active Edge Sites for Enhanced Electrocatalytic Hydrogen Evolution. *Adv. Mater.* **2013**, *25*, 5807–5813. [[CrossRef](#)]
134. Yu, D.; Nagelli, E.; Du, F.; Dai, L. Metal-Free Carbon Nanomaterials Become More Active than Metal Catalysts and Last Longer. *J. Phys. Chem. Lett.* **2010**, *1*, 2165–2173. [[CrossRef](#)]
135. Zhang, H.; Wang, Y.; Wang, D.; Li, Y.; Liu, X.; Liu, P.; Yang, H.; An, T.; Tang, Z.; Zhao, H. Hydrothermal Transformation of Dried Grass into Graphitic Carbon-Based High Performance Electrocatalyst for Oxygen Reduction Reaction. *Small* **2014**, *10*, 3371–3378. [[CrossRef](#)]
136. Zhang, H.; Chen, J.; Li, Y.; Liu, P.; Wang, Y.; An, T.; Zhao, H. Nitrogen-Doped Carbon Nanodots@Nanospheres as An Efficient Electrocatalyst for Oxygen Reduction Reaction. *Electrochim. Acta* **2015**, *165*, 7–13. [[CrossRef](#)]
137. Li, Y.; Zhao, Y.; Cheng, H.; Hu, Y.; Shi, G.; Dai, L.; Qu, L. Nitrogen-doped grapheme quantum dots with oxygen-rich functional groups. *J. Am. Chem. Soc.* **2012**, *134*, 15–18. [[CrossRef](#)]
138. Liang, J.; Jiao, Y.; Jaroniec, M.; Zhang Qiao, S. Sulfur and nitrogen dual-doped mesoporous grapheme electrocatalyst for oxygen reduction with synergistically enhanced performance. *Angew. Chem. Int. Ed. Engl.* **2012**, *51*, 11496–11500. [[CrossRef](#)] [[PubMed](#)]
139. Balakrishnan, M.; Batra, V.S.; Hargreaves, J.S.J.; Pulford, I.D. Waste Materials—Catalytic Opportunities: An Overview of the Application of Large Scale Waste Materials as Resources for Catalytic Applications. *Green Chem.* **2011**, *13*, 16–24. [[CrossRef](#)]
140. Mane, G.P.; Talapaneni, S.N.; Anand, C.; Varghese, S.; Iwai, H.; Ji, Q.; Ariga, K.; Mori, T.; Vinu, A. Preparation of Highly Ordered Nitrogen-Containing Mesoporous Carbon from a Gelatin Biomolecule and Its Excellent Sensing of Acetic Acid. *Adv. Funct. Mater.* **2012**, *22*, 3596–3604. [[CrossRef](#)]

Disclaimer/Publisher’s Note: The statements, opinions and data contained in all publications are solely those of the individual author(s) and contributor(s) and not of MDPI and/or the editor(s). MDPI and/or the editor(s) disclaim responsibility for any injury to people or property resulting from any ideas, methods, instructions or products referred to in the content.